

# Highly Modular Piano-Stool N-Heterocyclic Carbene Iron Complexes: Impact of Ligand Variation on Hydrosilylation Activity

Pamela V. S. Nylund, Nathalie C. Ségaud, and Martin Albrecht\*



Cite This: *Organometallics* 2021, 40, 1538–1550



Read Online

ACCESS |



Metrics & More

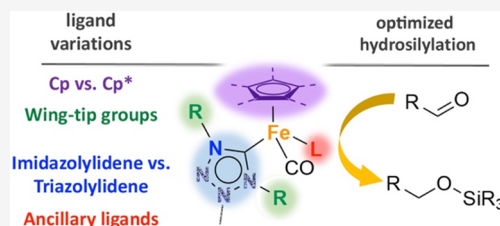


Article Recommendations



Supporting Information

**ABSTRACT:** The piano-stool configuration combined with N-heterocyclic carbene (NHC) ligation constitutes an attractive scaffold for employing iron in catalysis. Here, we have expanded this scaffold by installing a pentamethyl cyclopentadienyl (Cp\*) ligand as a strong electron donor compared to the traditionally used unsubstituted cyclopentadiene (Cp). Moreover, decarboxylation is introduced as a method to prepare these iron(II) NHC complexes, which avoids the isolation of air-sensitive free carbenes. In addition to the Cp/Cp\* variation, the complexes have been systematically modulated at the NHC scaffold, the NHC wingtip groups, and the ancillary ligands in order to identify critical factors that govern the catalytic activity of the iron center in the hydrosilylation of aldehydes. These modulations reveal the importance of steric tailoring and optimization of electron density for high catalytic performance. The data demonstrate a critical role of the NHC scaffold with triazolylidenes imparting consistently higher activity than imidazolylidenes and a correlation between catalytic activity and steric rather than electronic factors. Moreover, the implementation of steric bulk is strongly dependent on the nature of the NHC and severely limited by the Cp\* iron precursor. The best performing catalytic systems reach turnover frequencies, TOF<sub>max</sub>'s, of up to 360 h<sup>-1</sup> at 60 °C. Mechanistic investigations by <sup>1</sup>H NMR and *in situ* IR spectroscopies indicate a catalyst activation that involves CO release and aldehyde coordination to the [Fe(Cp)(NHC)I] fragment.



## INTRODUCTION

Iron is the second most abundant metal in the Earth's crust, easy to extract, and consequently cheap. Additionally, it is biologically relevant and known to be nontoxic to both humans and the environment. Despite these facts, iron was for a long time scarce in the catalytic literature compared to some of the more expensive, rare, and toxic metals in the periodic system. The application of iron as a molecular catalyst has been catching up with other metals over the last 20 years, however, and is now covering a plethora of organic reactions.<sup>1–3</sup> Hydrosilylation, one of the fields that has received much attention in iron catalysis during the past decades,<sup>4–8</sup> is a versatile methodology for the reduction of a variety of substrates under base-free conditions and without the need for highly reducing conditions as imparted by H<sub>2</sub> pressure.<sup>8–10</sup> In particular, hydrosilylation of alkenes is industrially important due to the increasing demand for silanes and siloxanes.<sup>11</sup>

In the past two decades, iron complexes have emerged as attractive hydrosilylation catalysts for alkenes in an approach to make industrial hydrosilylation more benign. While these systems normally deploy NN or NNN type ligands,<sup>12–16</sup> piano-stool iron complexes with N-heterocyclic carbene (NHC) ligands have demonstrated efficiency in the hydrosilylation of carbonyls rather than alkenes under fairly mild conditions.<sup>17–21</sup> These iron(II) complexes offer an excellent, cheap, and nontoxic alternative to systems based on noble metals such as rhodium, palladium, and platinum.<sup>8</sup> The

synthesis of NHC iron complexes is traditionally accomplished via the versatile free carbene route.<sup>22–25</sup> The need of base and inert conditions however poses limitations, and especially, NHCs with small wingtip groups risk rearrangement or decomposition under basic conditions.<sup>24–26</sup> Here, we present a new synthetic method to prepare NHC iron(II) piano-stool complexes. Moreover, we have used this and traditional methods to modularize NHC iron piano-stool complexes to evaluate the effects of variation in the cyclopentadiene (Cp) unit, the NHC scaffold, and the wingtip groups on catalytic hydrosilylation activity, demonstrating the importance of considering even slightly different catalysts depending on the substrate.

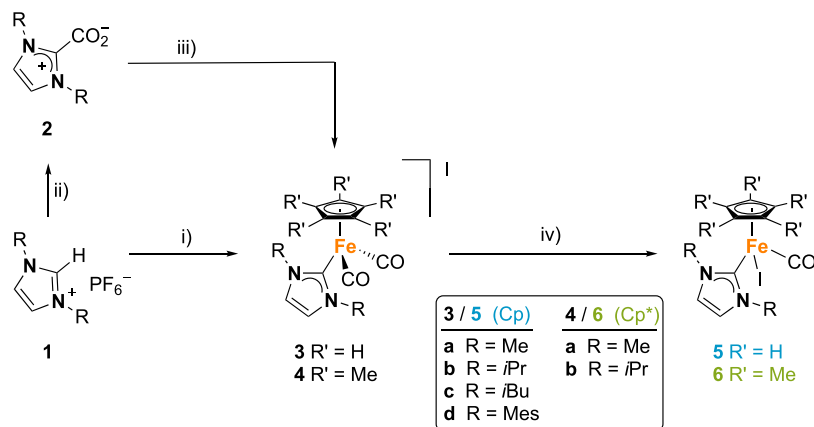
## RESULTS AND DISCUSSION

**Synthesis of Imidazole-Derived NHC Complexes.** The known imidazolylidene iron Cp complexes **3a**, **3b**, and **3d**<sup>22,23,27</sup> and the new complex **3c** were prepared by the established free base route involving the deprotonation of the corresponding imidazolium salts **1a–d** with KO<sup>t</sup>Bu followed

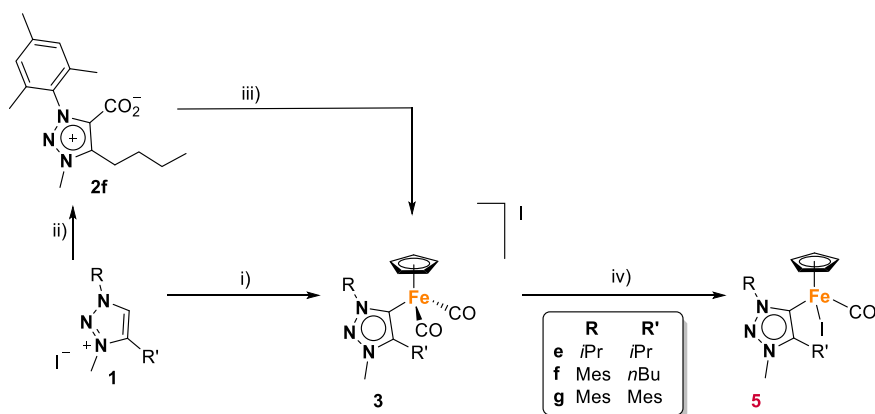
Received: April 1, 2021

Published: May 13, 2021



Scheme 1. Synthesis of Iron Imidazolyldene Complexes<sup>a</sup>

<sup>a</sup>Reagents and conditions: (i) KOtBu, THF, rt, 60 min, then [Cp(\*)Fe(CO)<sub>2</sub>I], toluene, rt, 16 h; (ii) KOtBu, THF, rt, 60 min, then CO<sub>2</sub>, toluene, rt, 1 h; (iii) [Cp(\*)Fe(CO)<sub>2</sub>I], toluene, 80 °C, 16 h; (iv) *hν*, CH<sub>2</sub>Cl<sub>2</sub>, 16 h.

Scheme 2. Synthesis of Iron Triazolyldene Complexes<sup>a</sup>

<sup>a</sup>Reagents and conditions: (i) KOtBu, THF, rt, 60 min, then [CpFe(CO)<sub>2</sub>I], toluene, rt, 16 h; (ii) KOtBu, THF, rt, 60 min, then CO<sub>2</sub>, toluene, rt, 1 h; (iii) [CpFe(CO)<sub>2</sub>I], toluene, 80 °C, 16 h; (iv) *hν*, CH<sub>2</sub>Cl<sub>2</sub>, 16 h.

by addition of the iron precursor [FeCp(CO)<sub>2</sub>I] (Scheme 1).<sup>22,23</sup> Using the pentamethyl cyclopentadienyl (Cp\*) precursor [FeCp\*(CO)<sub>2</sub>I] instead afforded complexes 4a and 4b in good yields. However, the analogous complex from imidazolium salt 1c with isobutyl wingtip groups did not form, suggesting higher steric congestion imparted by the Cp\* ligand as compared to the Cp system. Notably, two- and three-legged piano-stool complexes with mesityl-substituted NHC ligands were successfully prepared by the groups of Tatsumi and Song starting from the CO-free iron precursors [Cp\*FeN(SiMe<sub>3</sub>)<sub>2</sub>], [Cp\*FeCl(TMEDA)], and [FeCp\*(HMDS)] (TMEDA = Me<sub>2</sub>NCH<sub>2</sub>CH<sub>2</sub>NMe<sub>2</sub>, HMDS = N(SiMe<sub>3</sub>)<sub>2</sub>).<sup>28–31</sup>

Iron NHC complexes are generally prepared from the air and moisture sensitive free carbene, which requires inert conditions.<sup>32–34</sup> Here, we demonstrate that the decarboxylation method offers an attractive alternative for the synthesis of these iron complexes. While this strategy has previously been applied predominantly for platinum group metals,<sup>35</sup> its application to first-row transition metals is much rarer, mostly involves copper, and has never been applied to iron(II) precursors so far.<sup>36–40</sup> The reaction of the imidazolium carboxylate 2a with [FeCpI(CO)<sub>2</sub>] induced the release of CO<sub>2</sub> and afforded the known complex 3a in similar yields as via the deprotonation route (43% vs 58%, Scheme 1).<sup>23</sup>

Attractively, the metalation via decarboxylation proceeds in a distinct step that is not air or moisture sensitive and avoids the tedious isolation of the air-sensitive free carbene prior to transfer to the iron precursor. Likewise, the new Cp\* complexes 4a and 4b were also generated via decarboxylation of the imidazolium carboxylates 2a and 2b, respectively.<sup>35,41</sup>

The formation of the new cationic iron complexes 3c and 4a,b was supported in <sup>1</sup>H NMR spectroscopy by the expected relative integral ratio of the ligand signals and those of the Cp or Cp\* fragments at 5.31 and 1.83 ± 0.01 ppm, respectively, and by the characteristic Fe–C<sub>carbene</sub> resonance at δ<sub>C</sub> 162.5 ± 10.5 (Figures S1–S26). UV irradiation in CH<sub>2</sub>Cl<sub>2</sub> induced CO release and iodide coordination to form the neutral complexes 5 and 6. Ligand exchange was indicated by a characteristic color change from yellow to green as well as a diagnostic upfield shift of the Cp resonance in the <sup>13</sup>C NMR spectra from δ<sub>C</sub> ~88 to ~80 in complexes 5 and from ~99 to ~90 in the Cp\* complexes 6 as a consequence of the substitution of the π-accepting CO ligand with the stronger donating iodide (Figures S27–S38 and S39–S44, respectively). All <sup>1</sup>H and <sup>13</sup>C NMR shifts are in the same range as those of the related complexes.<sup>17,19,22</sup>

Analogous triazolyldene complexes were obtained from the triazolium salts 1e–g. The formation of previously reported

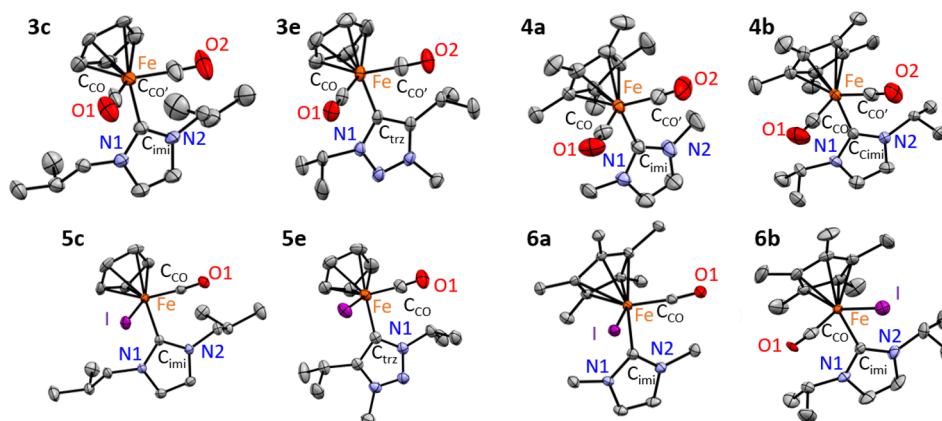


**Figure 1.** ORTEP representations (50% probability level) of the new cationic complexes **3c,e** and **4a,b** and the neutral analogues **5c,e** and **6a,b**. Hydrogen atoms and noncoordinating anions are omitted for clarity, and atom labeling is adjusted for consistency.

**Table 1.** Selected Bond Lengths [Å] and Angles [°] for cationic Cp complexes **3** and Cp\* complexes **4**<sup>a</sup>

complex ligand set	3a <sup>b</sup> imi/Cp	3b <sup>b</sup> imi/Cp	3c <sup>c</sup> imi/Cp	3e <sup>c</sup> trz/Cp	3f <sup>b</sup> trz/Cp	3g <sup>b</sup> trz/Cp	4a imi/Cp*	4b imi/Cp*
Fe–C <sub>imi/trz</sub>	1.969(6)	1.970(3)	1.965(6)	1.976(3)	1.974(3)	2.010(6)	1.979(4)	1.995(6)
Fe–C <sub>CO</sub>	1.777(5)	1.774(4)	1.769(9)	1.775(3)	1.765(4)	1.774(7)	1.762(5)	1.759(8)
Fe–C <sub>CO'</sub>	1.777(5)	1.780(3)	1.768(9)	1.767(3)	1.773(4)	1.767(6)	1.767(5)	1.772(8)
Fe–C <sub>centroid</sub>	1.731	1.716	1.752	1.718	1.724	1.727	1.743	1.738
C <sub>CO</sub> –Fe–C <sub>imi/trz</sub>	95.05(19)	94.2(1)	93.1(3)	94.07(12)	98.82(14)	99.26(3)	94.48(19)	93.6(3)
C <sub>CO'</sub> –Fe–C <sub>imi/trz</sub>	95.05(19)	94.4(2)	93.7(3)	92.58(12)	91.17(14)	97.54(6)	94.7(2)	95.2(3)
C <sub>CO</sub> –Fe–C <sub>CO'</sub>	93.4(3)	92.8(2)	90.5(4)	92.36(13)	92.24(17)	94.89(7)	93.1(2)	91.5(4)
C <sub>trz</sub> –Fe–C <sub>pcentroid</sub>	120.82	122.2	121.00	122.13	120.46	121.4(7)	122.92	123.50
N–C <sub>trz</sub> –Fe–C <sub>pcentroid</sub>	91.40	91.86	92.89	90.97	98.94	98.38	90.75	90.40

<sup>a</sup>imi = imidazolyldene; trz = triazolyldene. <sup>b</sup>Values obtained from ref 23 (3a and 3b) and ref 27 (3f and 3g). <sup>c</sup>Mixed occupation of anion site with I (82.3%) or PF<sub>6</sub> (17.7%).

**Table 2.** Selected Bond Lengths [Å] and Angles [°] for Neutral Cp Complexes **5** and Cp\* Complexes **6**

complex ligand set	5a <sup>d</sup> imi/Cp	5b <sup>d</sup> imi/Cp	5c imi/Cp	5d <sup>d</sup> imi/Cp	5e trz/Cp	5g <sup>d</sup> trz/Cp	6a imi/Cp*	6b imi/Cp*
Fe–C <sub>NHC</sub>	1.964(3)	1.972(5)	1.9652(19)	1.980(5)	1.990(4)	1.974(3)	1.970(3)	1.988(4)
Fe–C <sub>CO</sub>	1.749(3)	1.743(6)	1.7470(19)	1.641(9)	1.777(5)	1.747(3)	1.744(3)	1.736(5)
Fe–I	2.6548(3)	2.6597(8)	2.6428(3)	2.6445(8)	2.6813(6)	2.6391(4)	2.6582(4)	2.6452(6)
Fe–C <sub>centroid</sub>	1.730	1.726	1.727	1.742	1.744	1.722	1.743	1.743
C <sub>CO</sub> –Fe–C <sub>NHC</sub>	97.00(11)	95.2(3)	95.32(8)	101.2(5)	96.99(18)	99.48(13)	97.89(13)	97.80(17)
C <sub>NHC</sub> –Fe–I	92.35(7)	96.88(15)	92.98(5)	93.12	93.02(10)	92.16(7)	92.41(8)	95.46(11)
C <sub>CO</sub> –Fe–I	88.96(9)	85.3(2)	85.35(6)	86.5(3)	86.53(13)	89.91(10)	87.91(9)	86.75(15)
C <sub>NHC</sub> –Fe–C <sub>pcentroid</sub>	123.43	120.54	124.52	126.22	121.69	125.15	122.86	122.95
N–C <sub>NHC</sub> –Fe–C <sub>pcentroid</sub>	107.06	93.88	97.73	134.52	126.89	135.78	105.43	91.98

<sup>d</sup>Values obtained from ref 23 (5a and 5b), ref 22 (5d), and ref 27 (5g).

complexes **3f,g** proceeded smoothly via deprotonation with KO<sup>t</sup>Bu,<sup>27</sup> and the same methodology was applied to the triazolium salt **1e** to afford the new complex **3e** in moderate yields (Scheme 2). Notably, the iron triazolyldene complex **3f** was also accessible via the decarboxylation route from the new triazolium carboxylate **2f** and [FeCp(CO)<sub>2</sub>I] in similar yields as via the free carbene route (39% vs 42%). When irradiated, the cationic triazolyldene complexes **3e–g** transformed into the neutral complexes **5e–g**, which was indicated by a diagnostic color change from yellow to green as well as spectroscopic changes similar to those described for the imidazolyldene analogues, including an upfield shift of the Cp carbon signals from  $\delta_C$  88 to 80 ppm as well as a ~20 ppm downfield shift of the Fe–C<sub>carbene</sub> resonances. All new imidazolyldene and triazolyldene complexes were stable as solids in the ambient atmosphere but slowly decomposed in solution, indicated macroscopically by a gradual color change

to brown and the formation of a precipitate and microscopically by considerable broadening of the <sup>1</sup>H NMR signals.

Remarkably, the synthesis of the Cp\* analogues of **3e** and **3f** has failed in our hands. Neither the free carbene nor the decarboxylation route afforded the desired complexes. In an effort to increase the reactivity, *in situ* prepared cationic [FeCp\*(CO)<sub>2</sub>(THF)]OTf was used as an iron precursor<sup>42</sup> together with the free carbene from **1f**, though only paramagnetic products were obtained. In contrast, the triazolium salt **1e** with similar steric implications as the imidazolium salt **1b** gave, after deprotonation and reaction with [FeCp\*(CO)<sub>2</sub>I], the triazolyldene analogue of complex **4b** as suggested by the correct relative integral ratio of the ligand signals and the Cp–Me groups from a crude sample (Figure S45). Moreover, irradiation of the crude mixture induced the diagnostic color change to green; however, only traces of this complex were isolated, and we failed to develop

Table 3. Vibrational and Electrochemical Data for Cationic and Neutral Fe(II) Complexes 3–6

complex	NHC	wingtip	Cp <sup>(*)</sup>	$\nu_{\text{CO}}/\text{cm}^{-1}$ <sup>a</sup>	$E_{1/2}, (\Delta E) / \text{V}$ <sup>b</sup>
3a	imi	Me	Cp	2048, 2000	
3b	imi	<i>i</i> Pr	Cp	2050, 2003	
3c	imi	<i>i</i> Bu	Cp	2049, 2002	
3d <sup>c</sup>	imi	Mes	Cp	2050, 2006	
3e	trz	<i>i</i> Pr	Cp	2042, 1996	
3f <sup>d</sup>	trz	Mes, <i>n</i> bu	Cp	2041, 1994	
3g <sup>d</sup>	trz	Mes, Mes	Cp	2047, 2002	
3e	trz	<i>i</i> Pr	Cp	2042, 1996	
3f <sup>d</sup>	trz	Mes, <i>n</i> bu	Cp	2041, 1994	
4a	imi	Me	Cp <sup>*</sup>	2027, 1977	
4b	imi	<i>i</i> Pr	Cp <sup>*</sup>	2024, 1977	
5a	imi	Me	Cp	1932	+0.45 (0.10)
5b	imi	<i>i</i> Pr	Cp	1934	+0.41 (0.09)
5c	imi	<i>i</i> Bu	Cp	1934	+0.48 (0.09)
5d	imi	Mes	Cp	1938	+0.41 (0.09)
5e	trz	<i>i</i> Pr, <i>i</i> Pr	Cp	1928	+0.35 (0.10)
5f	trz	Mes, <i>n</i> bu	Cp	1935	+0.40 (0.10)
5g <sup>c</sup>	trz	Mes, Mes	Cp	1933	+0.34
6a	imi	Me	Cp <sup>*</sup>	1914	+0.19 (0.10)
6b	imi	<i>i</i> Pr	Cp <sup>*</sup>	1910	+0.15 (0.09)

<sup>a</sup>Measured in CH<sub>2</sub>Cl<sub>2</sub>. <sup>b</sup>Measured in CH<sub>2</sub>Cl<sub>2</sub> using 0.1 M [Bu<sub>4</sub>N][PF<sub>6</sub>] as supporting electrolyte, sweep rate of 100 mV s<sup>−1</sup>, referenced vs SSCE using Fc<sup>+</sup>/Fc as internal standard ( $E_{1/2} = +0.46$  V,  $\Delta E = 0.1$ ), in parentheses  $\Delta E = E_{\text{pa}} - E_{\text{pc}}$ . <sup>c</sup>From ref 22. <sup>d</sup>From ref 27.

synthetic methods to obtain this complex in sufficiently high quantities. Nonetheless, these experiments indicate that three-legged piano-stool Fe–Cp<sup>\*</sup> complexes with triazolydene complexes should, in principle, be accessible. Notably, Song and co-workers reported in 2020 a two-legged piano-stool Fe–Cp<sup>\*</sup> complex with a triazolydene ligand.<sup>31</sup>

**Structural Analyses.** Solid state X-ray crystal structures of representative examples of complexes 3–6 confirmed the piano-stool geometry and revealed bond lengths and angles in the expected range (Figure 1, Tables 1 and 2).<sup>22,23,27</sup> The Fe–C<sub>carbene</sub> bonds and the Fe–Cp distances are only marginally elongated (<0.025 Å) in the Cp<sup>\*</sup> complexes compared to their Cp analogues. Also, the relative orientation of the carbene ligand, determined by the N–C<sub>carbene</sub>–Fe–Cp<sub>centroid</sub> dihedral angle  $\theta$ , does not reveal any significant twists of the carbene in the cationic complexes 3 and 4 ( $\theta = 91.7^\circ \pm 1.3^\circ$ ) except for complex 3f and 3g ( $\theta = 98.9^\circ$  and  $98.4^\circ$ , respectively), which was attributed to steric constraints between the mesityl groups and the Cp protons.<sup>34</sup> The differences are more noticeable for the neutral complexes 5 and 6 ( $\theta$  between  $92^\circ$  and  $136^\circ$ ), suggesting a more flexible rotation. This flexibility may be facilitated by the smaller I–Fe–CO bond angle as compared to the CO–Fe–CO bond angle in the cationic analogues.

The steric implications of the Cp<sup>\*</sup> ligand were investigated by inspecting the shortest distance to NHC wingtip protons in each structure (Table S1). For the Cp complexes 3 and 5, the closest Cp–H...H<sub>NHC</sub> contacts were all between 2.25 and 2.74 Å with 3b displaying the shortest distance and 3c, the longest. The Cp<sup>\*</sup> complexes featured slightly shorter Cp–CH<sub>3</sub>...H<sub>NHC</sub> distances (2.12–2.35 Å). A comparison of Cp and Cp<sup>\*</sup> complexes with identical NHC ligand revealed a  $0.26 \pm 0.12$  Å

closer contact in the Cp<sup>\*</sup> complex. Close Cp–H...H<sub>NHC</sub> contacts were also identified in solution by Nuclear Overhauser effects (NOEs) between the Cp<sup>\*</sup> protons and the HC<sub>*i*Pr</sub> protons for 6b. Notably, no such NOE signals were detected in 5b with the same NHC ligand, yet a less bulky Cp instead of Cp<sup>\*</sup>. Interactions with the Cp ligand only became apparent when NHCs with bulkier wingtip groups were coordinated. For example, the Cp protons in complex 5f showed a NOE with both the mesityl–CH<sub>3</sub> and the N–CH<sub>2</sub> unit (Figures S51–S53). These results suggest that steric hindrance of the Cp<sup>\*</sup> ligand imposes more steric hindrance for bulky NHC ligands to coordinate to the iron center and rationalize the failure in preparing the Cp<sup>\*</sup> analogue of complex 3f (*vide supra*).

While the Cp complex 5a with small Me wingtip groups on the NHC ligand is fluxional due to rotation about the Fe–C<sub>NHC</sub> bond and requires low temperature (−20 °C) to reach decoalescence of the resonances in the <sup>1</sup>H NMR spectrum ( $\Delta G^\ddagger \sim 59$  kJ mol<sup>−1</sup>),<sup>23</sup> the analogous Cp<sup>\*</sup> complex 6a is more rigid and reveals a slow exchange limit spectrum with two nonequivalent N–CH<sub>3</sub> resonances at  $\delta_{\text{H}} = 4.04$  and 3.86, respectively (Figure S39).<sup>43</sup> In contrast, the signals from the *i*Bu wingtip groups of complex 5c were broad at room temperature, though they sharpened upon cooling to −20 °C (Figure S28, Table S2). From the coalescence temperature of these signals ( $T_{\text{coal}} = 298$  K) and the C<sub>imi</sub>–H resonance frequencies, a free energy of activation ( $\Delta G^\ddagger$ ) of  $58.0 \pm 1.0$  kJ mol<sup>−1</sup> was calculated for 5c. Complex 5e shows two rotamers in the <sup>1</sup>H NMR spectrum at −25 °C with a free energy of activation ( $\Delta G^\ddagger$ ) of  $60.5 \pm 1.0$  kJ mol<sup>−1</sup> (Figure S32, Table



S3). This higher energy compared to **5c** is commensurate with the larger steric demand of the wingtip groups in **5e**.

**Donor Properties of the Ligand Sets.** To determine the combined electron donor properties of the NHC ligand and the Cp(\*) moiety, the complexes were analyzed electrochemically and by IR spectroscopy. IR analysis revealed the characteristic symmetric and asymmetric bands  $\nu_s = 2037 \pm 12 \text{ cm}^{-1}$  and  $\nu_{as} = 1990 \pm 13 \text{ cm}^{-1}$  for the cationic bis-carbonyl complexes **3** and **4** and a single absorption in the 1910–1935  $\text{cm}^{-1}$  range for the neutral monocarbonyl complexes **5** and **6** (Table 3). Triazole-derived NHCs induce generally a  $6 \pm 1 \text{ cm}^{-1}$  lower energy vibration than imidazolylidenes (cf. **5b** vs **5e** and **5d** vs **5g**) in line with the increased electron donor properties of triazolylidenes.<sup>44</sup> The wingtip group modification had minor implications for both imidazole- and triazole-derived carbenes in the cationic systems yet induced some variation in the neutral complexes ( $\Delta\nu_{\text{max}} = 7 \text{ cm}^{-1}$ , cf. **5f** vs **5e** and **6a** vs **6b**). The most substantial shift was noted upon replacing the Cp ligand for Cp\* ( $\Delta\nu = 22 \pm 4 \text{ cm}^{-1}$ ), indicating a major effect of the stronger electron donating Cp\* ligand (cf. **3a,b** vs **4a,b**, and **5a,b** vs **6a,b**).

Further insights into the electronic modulation of these complexes were gained by electrochemical analysis. While the cationic complexes did not show any oxidation process up to 1.4 V vs SSCE, the neutral complexes **5** and **6** feature a reversible oxidation in cyclic voltammetry (CV; Figure S54). The half-wave potentials shift only slightly by <90 mV upon changing the wingtip group (Table 3). The substitution of the imidazolylidene scaffold for a triazolylidene lowered the oxidation potential by  $0.065 \pm 0.05 \text{ V}$  (cf. **5b,d** vs **5e,g**), and the exchange of Cp for Cp\* had again the largest effect and shifted the redox potential by 0.27 V (cf. **5a,b** vs **6a,b**). These data are in good agreement with the trends deduced from IR spectroscopy and indicate that the Cp/Cp\* modulation is 2–3 times larger than the swap of the NHC from imidazolylidene to triazolylidene. Wingtip modification is nonlinear, and the electron-donating character of secondary alkyl groups is counterbalanced by steric effects, especially with Cp\* ligands. According to both analyses, complex **6b** features the most electron rich iron center with decreasing electron-density along the series **6b** > **6a** > **5e** > **5g** > **5f** > **5d** > **5b** > **5a** > **5c**. These effects are displayed in Figure 2 for representative examples featuring a variable wingtip group, NHC scaffold, and Cp vs Cp\* ligand, respectively.

#### Catalytic Hydrosilylation of Carbonyl Compounds.

The impact of the broad electronic tunability of these iron complexes **5** and **6** was evaluated in the reduction of carbonyl compounds via hydrosilylation.<sup>18,27</sup> 4-Nitrobenzaldehyde was employed as a benchmark substrate and  $\text{PhSiH}_3$ , as hydrosilylation agent; yields were calculated after the Si–O bond cleavage with  $\text{Bu}_4\text{NF}$  (Table 4). Very distinct time–conversion profiles were observed, which indicate a profound influence of the ligand set on the catalytic activity (Figure 3). A comparison of the catalytic performance revealed some general trends. First, the introduction of a Cp\* spectator ligand instead of Cp is detrimental to catalytic activity and leads to considerably slower conversion (cf. complexes **5a** and **6a**, turnover frequency ( $\text{TOF}_{\text{max}}$ ) = 30 vs 20  $\text{h}^{-1}$ , entries 1 and 8) though this is less pronounced when the carbene contains *i*Pr instead of methyl wingtip groups (**5b** vs **6b**, entries 2 and 9). Second, the replacement of the carbene scaffold from imi to trz reduces the reaction time and enhances the catalytic performance considerably (cf. complexes **5b** and **5e**,  $\text{TOF}_{\text{max}}$  = 50 vs 160

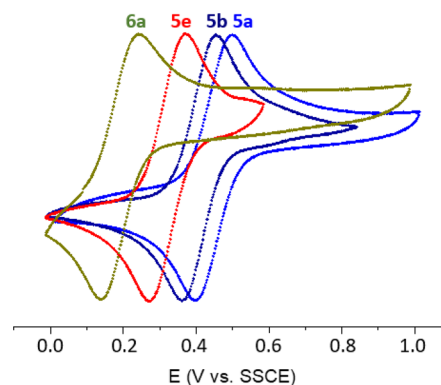


**Figure 2.** Normalized cyclic voltammograms of representative complexes **5a**, **5b**, **5e**, and **6a** measured in  $\text{CH}_2\text{Cl}_2$ , 0.1 M  $[\text{Bu}_4\text{N}]\text{PF}_6$ , potential in V vs SSCE and referenced to  $\text{Fc}^+/\text{Fc}$  ( $E_{1/2} = +0.46 \text{ V}$ ,  $\Delta E = 0.1 \text{ V}$ ) or decamethyl ferrocene ( $E_{1/2} = +0.11 \text{ V}$ ,  $\Delta E = 0.1 \text{ V}$ ), 100  $\text{mV s}^{-1}$  sweep rate.

$\text{h}^{-1}$ , entries 2 and 5; complexes **5d** and **5g**,  $\text{TOF}_{\text{max}} = 140$  vs 230  $\text{h}^{-1}$ , entries 4 and 7) with previously reported complex **5g** as the most active complex in this series.<sup>27</sup> Third, wingtip modulations have a marked effect on turnover frequencies, which increase as follows:  $\text{Me} < \text{iPr}, \text{iBu} < \text{Mes}$  for the imi series (entries 1–4) and similarly  $\text{iPr}, \text{iPr} < \text{nBu}, \text{Mes} < \text{Mes}, \text{Mes}$  in the trz series (entries 5–7). The complexes show varying induction times ranging from 10 up to 90 min, suggesting that the active catalyst is formed *in situ*.

Notably, there is no clear correlation between the catalytic performance and the redox potential as a proxy for the donor properties of the ligand set (Figure 4a). While there is a good trend in the Cp series with more donating NHCs increasing the activity, this trend is not confirmed by the imi/Cp\* series, which should provide much higher activity than that observed if the electron density at iron is indeed the decisive factor for catalytic performance.

A more stringent trend was revealed when the catalytic activity of the complexes was correlated with the steric influence of the NHC ligand (Figure 4b) as deduced from the percentage buried volume ( $\%V_{\text{bur}}$ ) calculated with the SambVca software (Figure S55).<sup>45</sup> Accordingly, even a slight increase of the percentage buried volume leads to a higher catalyst performance with the mesityl-substituted NHCs ( $V_{\text{bur}} = 30\text{--}31.2\%$ ,  $\text{TOF}_{\text{max}} = 180\text{--}230 \text{ h}^{-1}$ ) performing better than the analogues with alkyl wingtip groups ( $V_{\text{bur}} = 25.6\text{--}27.4\%$ ,  $\text{TOF}_{\text{max}} = 30\text{--}160 \text{ h}^{-1}$ ). While these steric parameters appear to be the dominant factor for tailoring catalytic activity, the electronic factors allow for fine-tuning the activity with trz systems outperforming the imi analogues (cf. **5b** vs **5e** and **5d** vs **5g**).

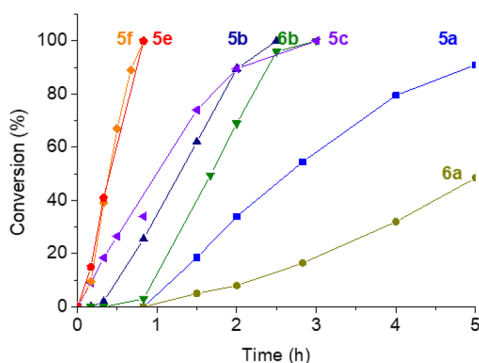
In order to probe the steric implications of the Cp\* spectator ligand, different substrates with varying spatial requirements were evaluated, viz. butyraldehyde as a small substrate and *o*-tolualdehyde as a bulky substrate (Table 5, Figure S56). Except for complexes **5a** and **6a** with methyl-substituted NHCs, catalytic activities increased when changing the substrate from 4-nitrobenzaldehyde to either of these two aldehydes (Table 5). In addition, turnover frequencies were generally higher for the bulkier *o*-tolualdehyde than for butyraldehyde. Interestingly, the exchange of Cp for Cp\* generally induced an improved catalytic activity toward both the smaller butyraldehyde (relative to nitrobenzaldehyde) and the sterically more demanding tolualdehyde (cf. complexes **5b**

Table 4. Hydrosilylation of 4-Nitro Benzaldehyde by Iron(II) Complexes 5–6<sup>a</sup>

1) [Fe], 1 mol %  
PhSiH<sub>3</sub>, DCE 60 °C  
2) TBAF, CDCl<sub>3</sub>

entry	[Fe]	conversion (%) <sup>b</sup>	yield (%) <sup>c</sup>	induction (min)	time (h)	TOF <sub>max</sub> (h <sup>-1</sup> )
1	<b>5a</b>	100	89	90	21	30
2	<b>5b</b>	100	93	<20	2.5	50
3	<b>5c</b>	100	90	<10	3	50
4 <sup>d</sup>	<b>5d</b>	97	n.d.	30	1	140
5	<b>5e</b>	100	99	10	0.83	160
6	<b>5f</b>	100	88	10	0.83	180
7 <sup>d</sup>	<b>5g</b>	99	n.d.	30	1	230
8	<b>6a</b>	100	94	90	21	20
9	<b>6b</b>	100	95	50	3	50
10	[FeCp*(CO) <sub>2</sub> I]	<2	<2	-	21	-
11	<b>1b</b>	<2	<2	-	21	-

<sup>a</sup>General conditions: substrate (0.5 mmol), PhSiH<sub>3</sub> (0.6 mmol), [Fe] complex (5 μmol, 1 mol %), C<sub>6</sub>Me<sub>6</sub> as internal standard (50 μmol), 1,2-dichloroethane (DCE; 2.5 mL), 60 °C. <sup>b</sup>Conversion determined by <sup>1</sup>H NMR spectroscopy as an average of at least two runs. <sup>c</sup>Spectroscopic yield after alcohol deprotection. <sup>d</sup>From ref 27.



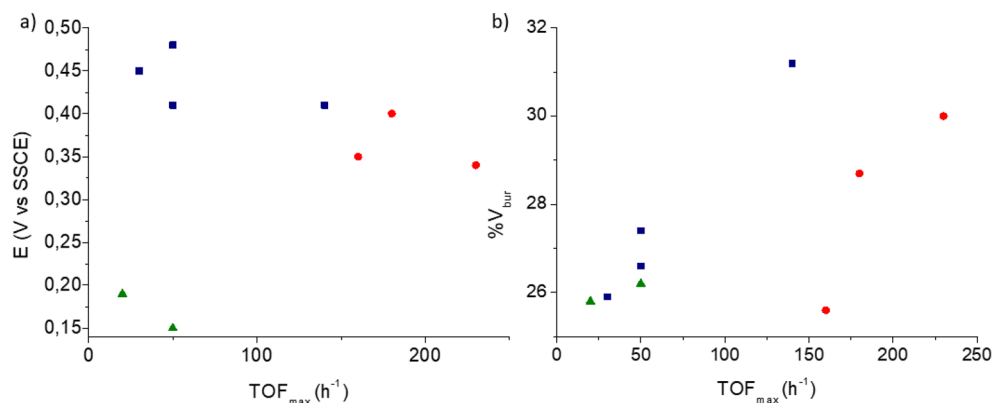
**Figure 3.** Time–conversion profile of the hydrosilylation of 4-nitrobenzaldehyde by iron(II) complexes 5–6 (conditions as in Table 4).

and **6b**, TOF<sub>max</sub> = 70–80 vs 160–180 h<sup>-1</sup>; entries 2, 6, 8, and 12). In both the Cp and Cp\* analogues, the imidazolylidene ligand with the *i*Pr wingtip group (**5b** and **6b**) is favorable in the hydrosilylation catalysis over the methyl analogue (**5a** and **6a**; TOF<sub>max</sub> = 10–20 vs 70–80 h<sup>-1</sup> (**5a** vs **5b**), 6–20 vs 160–180 h<sup>-1</sup> (**6a** vs **6b**), entries 1, 2, 5–8, 11, and 12). These results suggest that the sterically hindered catalysts with a Cp\*

spectator ligand do not discriminate bulkier substrates compared to their Cp analogues with a sterically better available iron center. The choice of Cp vs Cp\* is therefore substrate dependent and needs to be evaluated for determining the best performing catalyst system. As shown above for nitrobenzaldehyde, also for the butyraldehyde and tolualdehyde, the TOF<sub>max</sub> correlates reasonably well with steric ligand parameters and much less with the ligand electronics (Figure S57a,b) though, again, the trz ligands outperform the imi series.

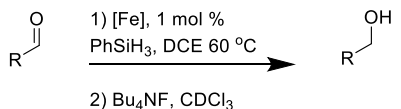
While there was no steric discrimination observed between tolualdehyde and butyraldehyde, a steric bias can be deduced, however, from experiments using very bulky substrates. Thus, neither mesityl benzaldehyde nor *o*-tolyl methyl ketone are converted even when using the most potent trz/Cp complex **5f**. Likewise, benzylacetate is not hydrosilylated under these conditions.

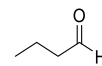
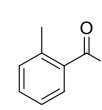
**Mechanistic Studies.** While previous work disclosed a variety of mechanistically diverse catalytic cycles,<sup>27,46–50</sup> we aimed here to shed some light on the mode of activation of these carbene iron catalysts in hydrosilylation. Therefore, a set of stoichiometric experiments was conducted as well as some tailored modifications of the catalyst precursor in order to



**Figure 4.** (a) Plot of oxidation potentials ( $E_{1/2}$ ) vs TOF<sub>max</sub> for the catalytic hydrosilylation of 4-nitrobenzaldehyde; (b) correlation of buried volume (%V<sub>bur</sub>) with TOF<sub>max</sub>. Color code: imi/Cp ligand set in blue, trz/Cp ligand set in red, and imi/Cp\* ligand set in green.

Table 5. Hydrosilylation of Butyr- and Toluvaldehyde by Iron(II) Complexes 5 and 6<sup>a</sup>

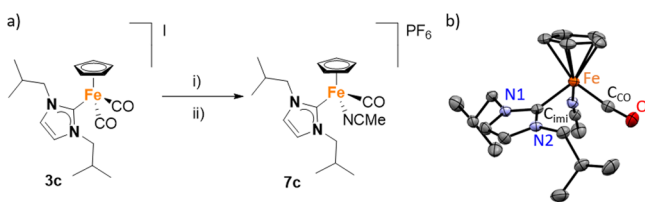


entry	complex	substrate	conversion (%) <sup>b</sup>	yield (%) <sup>c</sup>	induction (min)	time (h)	TOF <sub>max</sub> (h <sup>-1</sup> )
1	5a		100	79	80	24	20
2	5b		96	90	25	7	70
3	5e		100	99	10	1	240
4	5f		100	99	15	1.5	290
5	6a		56	45	80	45	6
6	6b		100	97	<20	1	160
7	5a		97	90	50	75	10
8	5b		100	93	20	3	80
9	5e		100	88	10	0.70	270
10	5f		100	99	25	1	360
11	6a		100	85	120	24	20
12	6b		100	99	20	2.3	180

<sup>a</sup>General conditions: substrate (0.5 mmol), PhSiH<sub>3</sub> (0.6 mmol), [Fe] complex (5 μmol, 1 mol %), C<sub>6</sub>Me<sub>6</sub> (50 μmol) as internal standard, DCE (2.5 mL), 60 °C. <sup>b</sup>Conversion determined by <sup>1</sup>H NMR spectroscopy as an average of at least two runs. <sup>c</sup>Spectroscopic yield determined for silylated butanol and deprotected 2-methyl-benzylalcohol, respectively.

facilitate the activation process. When the electronic saturation of the iron complexes 5 and 6 due to their 18 electron configuration is considered, η<sup>5</sup>-to-η<sup>3</sup> Cp ring slippage<sup>51</sup> or the dissociation of an ancillary ligand constitute plausible activation pathways. The latter hypothesis is supported by earlier work that demonstrated that cationic complexes akin to 3 and 4 require UV irradiation to become active hydrosilylation catalysts.<sup>18</sup>

**Probing Iodide Dissociation.** When complex 5f was dissolved in MeCN, the color gradually darkened and turned red within 10 min with concomitant formation of a second species according to <sup>1</sup>H NMR spectroscopy (Figure S58). This change was reversible and was attributed to iodide dissociation and solvent coordination, a process that may also be potentially relevant for catalyst activation. To investigate the relevance of iodide coordination, complex 7c was prepared in which the iodide was replaced with MeCN as a potentially better leaving group (Scheme 3). This complex was readily

Scheme 3. Synthesis and ORTEP Plot of Complex 7c<sup>a</sup>

<sup>a</sup>50% probability, all hydrogen atoms and non-coordinating PF<sub>6</sub><sup>-</sup> anions omitted for clarity. Reagents and conditions: (i) AgPF<sub>6</sub>, CH<sub>2</sub>Cl<sub>2</sub>, room temperature, 1 h; (ii) hν, MeCN, 1 h.

obtained from the dicarbonyl precursor 3c via AgPF<sub>6</sub>-mediated anion exchange followed by UV irradiation in MeCN. The coordination of MeCN was confirmed by a characteristic singlet at δ<sub>H</sub> = 2.28 in the <sup>1</sup>H NMR spectrum (Figure S46).

Complex 7c catalyzed the hydrosilylation of 4-nitrobenzaldehyde under standard conditions, though considerably slower than its iodide analogue 5c. It required 70 h to reach 68% conversion compared to full conversion in 3 h with 5c

(Table S9). In an attempt to generate a putative catalytic iron alkoxide or iron hydride intermediate, complex 7c was used as a catalyst precursor in the presence of LiOiPr or NaBH<sub>4</sub> as additives.<sup>49</sup> Neither of these additives improved the catalytic activity and, to the contrary, resulted in lower conversions. Also, stoichiometric <sup>1</sup>H NMR experiments did not lead to a defined complex and in the presence of LiOiPr only revealed broadening of the signals (Figure S59). Likewise, the addition of 0.6 equiv of I<sub>2</sub> (relative to the iron complex) as a mild oxidizing agent to access a putative iron(III) species only lowered the catalytic performance. These data therefore point to some relevance of iodide coordination for imparting catalytic activity.

**Monitoring Stoichiometric Experiments.** The exposure of complex 5f to 2 equiv of 4-nitrobenzaldehyde in CD<sub>2</sub>Cl<sub>2</sub> at 60 °C for 30 min induced the formation of a minor new set of aromatic signals at 8.10 and 7.49 ppm of about 5% of the intensity compared to nitrobenzaldehyde (Figures S60 and S61). The addition of 4 equiv of PhSiH<sub>3</sub> led to the complete consumption of 4-nitrobenzaldehyde within 10 min (Figure S60c,d). When a stoichiometric mixture of 4-nitrobenzaldehyde and complex 5f in DCE-*d*<sub>4</sub> was heated for 3 h, an almost full depletion of the aldehyde signals was noted (Figure S62).<sup>52</sup> These changes may point to the formation of a paramagnetic species, such as an iron-alkoxy complex, though these events are clearly outside the catalytic time regime. Nonetheless, these data suggest that the substrate is interacting with the complex but that the resulting species is either not stable enough to be isolated or not detectable by <sup>1</sup>H NMR spectroscopy. Notably, complex 5f on its own is stable in refluxing CD<sub>2</sub>Cl<sub>2</sub> for >2 h and degrades slowly in DCE-*d*<sub>4</sub> yet without the formation of any new signals (Figures S63 and S64).

The complementary reaction of complex 5f with 3 equiv of PhSiH<sub>3</sub> at 60 °C in the absence of aldehyde substrate induced spectral changes only after 20 min with the appearance of a new set of signals and in particular a weak signal at -14.29 ppm (Figures S65 and S66), suggesting the formation of small quantities of an iron hydride species (<5%).<sup>53,54</sup> The main species in the spectrum remained 5f, and this was visibly supported by the bright green color of the solution. The

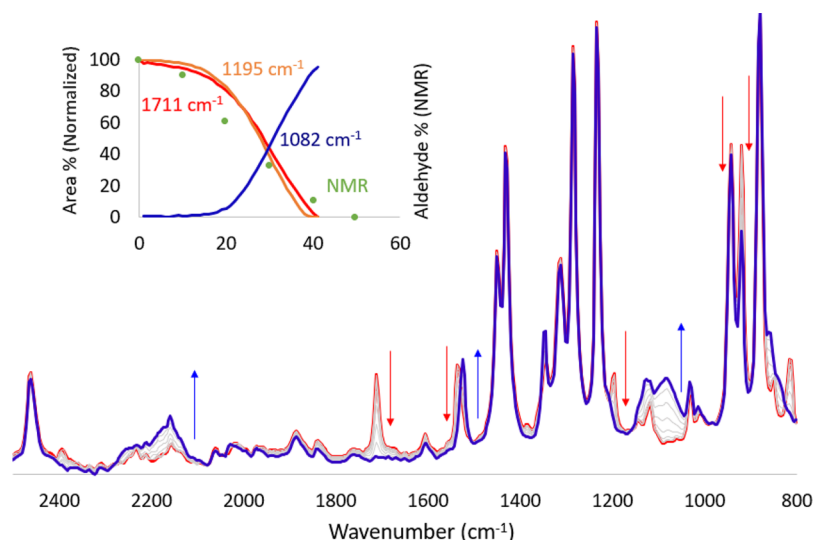


**Figure 5.** *In situ* FT-IR spectra recorded during hydrosilylation of 4-nitrobenzaldehyde with **5f** as catalyst under standard conditions (Table 4). Changes over time in 5 min intervals (red at 0 h and blue at 40 min); red arrows indicate the change of signal intensities. Inset: Catalytic profile of two catalytic reactions with conversions determined by  $^1\text{H}$  NMR spectroscopy (green circles) and by IR spectroscopy from changes at 1195 and 1711  $\text{cm}^{-1}$  (signals of 4-nitrobenzaldehyde, amber and red traces) and 1082  $\text{cm}^{-1}$  (attributed to the Si–O band in the product, blue trace).

addition of 2 equiv of 4-nitrobenzaldehyde resulted in its full consumption within 10 min (Figure S65c,d) and the disappearance of the hydride resonance. Upon addition of an extra 2 equiv of aldehyde, again some 60% was consumed within 10 min (Figure S65e), indicating full consumption of the silane and pointing to an iron species in solution that remains catalytically active. The presence of signals due to **5f** after these three turnovers revealed that only a small fraction of the precatalyst was transformed to the active species. Notably, the iron complex in the presence of only  $\text{PhSiH}_3$  was stable far beyond the induction period typically observed in catalytic runs (up to 25 min for complex **5f**, cf. Tables 4 and 5, Figure S67). Only extended incubation of **5f** at 60  $^\circ\text{C}$  led to a color change from green to yellow with a 50% decrease of the signals of the original iron complex after 16 h (Figure S67). Concomitantly, the  $^1\text{H}$  NMR resonance of  $\text{PhSiH}_3$  at 4.15 ppm decreased to  $\sim 5\%$  and new singlets appeared at 5.02 and 5.19 ppm together with downfield shifted aromatic signals, which were attributed to reshuffled phenylsilane<sup>55,56</sup> and siloxane species; the latter presumably formed due to fortuitous moisture or oxygen (Figure S68).

The combined results from these NMR studies suggest the formation of a pre-equilibrium either between the iron complex and the silane to form an iron hydride as the putative active species or involving the iron complex and the aldehyde to form an iron substrate adduct. In either case, there is a strong preponderance toward the dissociated species, i.e., the starting materials. Notably, such a pre-equilibrium situation may rationalize the observed induction periods under catalytic conditions.

**In Situ Reaction Monitoring.** The CO functionalities in both the complex and the aldehyde substrate provided a diagnostic handle to use ReactIR spectroscopy for investigating the catalyst activation and performance *in situ*. A catalytic run under standard conditions with complex **5f** revealed a gradual decrease of the C=O stretch vibration of the 4-nitrobenzaldehyde at 1711 and 1195  $\text{cm}^{-1}$  and a concomitant increase of a broad band at 1082  $\text{cm}^{-1}$  attributed to the C–O–Si unit indicative for the formation of the hydrosilylated

products (Figure 5). New phenylsilane products are suggested by the appearance of a broad band around  $\nu_{\text{SiH}} = 2160 \text{ cm}^{-1}$ .<sup>57</sup> The plot of the normalized intensity changes over time yields similar rates as deduced from  $^1\text{H}$  NMR monitoring of a parallel reaction (inset of Figure 5).

Catalyst activation was monitored in a set of stoichiometric experiments and corroborated the conclusions deduced from NMR spectroscopic analyses. The interaction of complexes **5c** or **5f** with 4-nitrobenzaldehyde in a 1:1 molar ratio resulted in a linear decrease of the carbonyl vibration bands of the complex and aldehyde at 1935 and 1711  $\text{cm}^{-1}$ , respectively, and the full disappearance within 40 min (Figures S72 and S73), strongly suggesting an interaction between the substrate and the catalyst through CO dissociation from the iron coordination sphere.<sup>58</sup> A similar process has been established for the Shvo catalyst where CO dissociation is more favorable than  $\eta^5/\eta^3$  ring slippage.<sup>59,60</sup>

Stoichiometric experiments with complex **5f** and  $\text{PhSiH}_3$  (1 equiv) showed a substantially slower transformation of **5f** than those in the presence of aldehyde under otherwise identical conditions (20% in 1 h; Figure S75). The addition of 1 equiv of 4-nitrobenzaldehyde led to a full disappearance after 45 min of the CO band of the complex and full consumption of the substrate, together with almost a 50% decrease of the phenylsilane. The time regime of these experiments suggests that the iron complex has a much higher affinity for the aldehyde and indicates that (reversible) CO dissociation and aldehyde coordination constitute a plausible catalyst activation pathway. Of course, the currently available data cannot rule out a Curtin-Hammett scenario with a catalytically irrelevant pre-equilibrium aldehyde coordination and parallel formation of an iron hydride as the active species present in too low quantities to be detected by ReactIR. We note however that aldehyde coordination and conversion have a strong influence since earlier work in our group demonstrated that the hydrosilylation of ketones is hampered unless the catalytically active species is formed by spiking the reaction with some aldehyde.<sup>27</sup>

In support of the mechanistic scenario involving ketone coordination in the catalyst activation step, an additional



catalytic experiment was conducted in which complex **6b** was prestirred with 4-nitrobenzaldehyde for 1 h. The addition of  $\text{PhSiH}_3$  initiated catalytic turnover immediately without any activation period, and conversion was complete within 60 min according to  $^1\text{H}$  NMR monitoring (Figure S76). In comparison, without prestirring, an induction time of some 40 min was observed with this catalyst system, indicating that aldehyde coordination to iron is relevant. In contrast, the preactivation of complex **6b** with  $\text{PhSiH}_3$  resulted in much slower conversion, requiring 110 min to reach completion (Figure S76). These data lend strong support to a catalyst activation involving CO ligand displacement by the aldehyde substrate rather than formation of an initial iron hydride species from the iron complex and the silane.

## CONCLUSION

This work extends the diversity of piano-stool NHC iron complexes and includes variation of the NHC scaffold, the wingtip group, and ancillary ligands as well as modulation of the Cp ligand with the stronger donating  $\text{Cp}^*$  analogue. Variability was also implemented on the synthetic level by introducing decarboxylation, so far unprecedented for iron(II) precursors, for preparing both imidazolyldene and triazolyldene piano-stool iron complexes. The application of these iron complexes with diverse ligand sets in the catalytic hydrosilylation of aldehydes revealed a clear trend in activity that depends strongly on the NHC scaffold ( $\text{trz} > \text{imi}$ ) and revealed a good correlation with steric parameters as defined by the %  $V_{\text{bur}}$ . Notably, the choice of Cp vs  $\text{Cp}^*$  ligand may be substrate dependent; for example, the activity increase is opposite for nitrobenzaldehyde and butyraldehyde. Mechanistic investigations provide strong support for a catalyst activation that involves displacement of the CO ligand with the aldehyde substrate. Such a process rationalizes the critical role of the substrate in catalyst optimization and also the low activity of these complexes toward ketones. Moreover, it validates the need for a high modularity of the ligand sets in these piano-stool iron(II) complexes as demonstrated in this work. The option to vary virtually all parameters, from carbene scaffold to wingtip sterics and electronics, ancillary ligand, Cp substitution pattern, and counterions around the iron(II) center, will also offer opportunities for exploring further catalytic applications beyond hydrosilylation.

## EXPERIMENTAL SECTION

**General Comments.** Toluene, THF,  $\text{CH}_2\text{Cl}_2$ ,  $\text{Et}_2\text{O}$ , and hexane were dried by passage through solvent purification columns. 1,2-Dichloroethane was dried over 4 Å molecular sieves and degassed with argon. All other reagents were commercially available and used without further purification. Metalation reactions and the purification of complexes were carried out under an inert nitrogen atmosphere using standard Schlenk techniques. The synthesis of complexes **3a**, **3b**, **3d**, **3f**, **3g**, **5a**, **5b**, **5d**, **5f**, and **5g**<sup>22,23,27</sup> have been reported elsewhere, and the synthesis of all ligands is provided in the Supporting Information. NMR spectra were measured at 25 °C on Bruker spectrometers operating at 300 or 400 MHz ( $^1\text{H}$  NMR) and 75 or 101 MHz ( $^{13}\text{C}\{^1\text{H}\}$  NMR), respectively. Chemical shifts ( $\delta$  in ppm, coupling constants  $J$  in Hz) were referenced to residual solvent resonances downfield to  $\text{SiMe}_4$ . Assignments were made based on homo- and heteronuclear shift correlation spectroscopy. The purity of bulk samples of the complexes has been established by NMR spectroscopy and by elemental analysis, which was performed at the University of Bern Microanalytic Laboratory by using a Thermo Scientific Flash 2000 CHNS-O elemental analyzer. High-resolution

mass spectrometry was carried out with a Thermo Scientific LTQ Orbitrap XL instrument (ESI-TOF). IR spectra were recorded on a Jasco 4700 FT-IR instrument in  $\text{CH}_2\text{Cl}_2$  solution at 1  $\text{cm}^{-1}$  resolution. Time-resolved online MCT FT-IR spectra were recorded on a ReactIR 15 Instrument (Mettler Toledo) equipped with a diamond probe (DiComp, optical range of 3000–650  $\text{cm}^{-1}$ ). For online monitoring, the diamond probe was introduced into a 10 mL Schlenk containing the reaction mixture, and spectra were recorded at specific times. The experiments were run under nitrogen conditions. UV irradiation was carried out using a UVP Blak-Ray B-100AP lamp. Cyclic voltammetry measurements were carried out using a Metrohm Autolab Model PGSTAT101 potentiostat employing a gastight three-electrode cell under an argon atmosphere. A platinum disk with 7.0  $\text{mm}^2$  surface area was used as the working electrode and polished before each measurement. The reference electrode was Ag/AgCl; the counter electrode was Pt foil.  $\text{Bu}_4\text{NPF}_6$  (0.1 M) in dry  $\text{CH}_2\text{Cl}_2$  was used as supporting electrolyte with analyte concentrations of approximately 1 mM. The ferrocenium/ferrocene ( $\text{Fc}^+/\text{Fc}$ ) redox couple was used as an internal reference ( $E_{1/2} = 0.50$  V vs SSCE).<sup>61</sup>

### General Procedure for the Preparation of Complexes **3** and **4**.

**Method A.** The imidazolium/triazolium salt (1 equiv) and  $\text{KOtBu}$  (1.2 equiv) were suspended in dry THF (10 mL). After 1 h of stirring at room temperature, the THF was removed under reduced pressure and the free carbene was extracted in dry toluene ( $2 \times 6$  mL); the resulting suspension was filtered into a dry toluene (3 mL) solution of  $[\text{CpFe}(\text{CO})_2\text{I}]$  or  $[\text{Cp}^*\text{Fe}(\text{CO})_2\text{I}]$  (0.9 equiv). The resulting mixture was stirred at room temperature under the exclusion of light for 16 h. The precipitate was collected by filtration, washed with toluene ( $2 \times 5$  mL), extracted with  $\text{CH}_2\text{Cl}_2$ , and dried *in vacuo* to yield the crude product as a light-sensitive material, which hampered further purification.

**Method B.** The azolium carboxylate **2** and iron precursor were suspended in dry toluene (6 mL) and stirred at 80 °C for 16 h under the exclusion of light. After cooling to room temperature, the precipitate was collected by filtration and purified as described in Method A.

**Synthesis of **3a**.** According to Method B, complex **3a** was afforded as a yellow powder (65 mg, 43%) by starting from **2a** (52 mg, 0.38 mmol) and  $[\text{CpFe}(\text{CO})_2\text{I}]$  (114 mg, 0.38 mmol). Analytical data agree with those reported for this compound.<sup>23</sup>

**Synthesis of **3c**.** According to Method A, complex **3c** was afforded as a yellow powder (308 mg, 75%) by starting from **1c** (334 mg, 1.02 mmol),  $\text{KOtBu}$  (155 mg, 1.28 mmol), and  $[\text{CpFe}(\text{CO})_2\text{I}]$  (259 mg, 0.85 mmol). Single crystals suitable for X-ray diffraction were obtained by the slow diffusion of  $\text{Et}_2\text{O}$  to a  $\text{CH}_2\text{Cl}_2$  solution of the complex.

$^1\text{H}$  NMR (400 MHz,  $\text{CD}_2\text{Cl}_2$ ):  $\delta$  7.38 (br, 2H,  $\text{H}_{\text{im}}$ ), 5.31 (s, 5H, Cp), 4.00 (d,  $J = 7.8$  Hz,  $\text{CH}_2$ ), 2.22 (sept,  $J = 7.0$  Hz, 2H, CH), 1.02 (d,  $J = 6.6$  Hz, 12H,  $\text{CH}_3$ ).  $^{13}\text{C}\{^1\text{H}\}$  NMR (101 MHz,  $\text{CD}_2\text{Cl}_2$ ):  $\delta$  211.81 (CO), 164.47 ( $\text{C}_{\text{im}}-\text{Fe}$ ), 125.54 ( $\text{C}_{\text{im}}-\text{H}$ ), 87.66 (Cp), 59.20 ( $\text{CH}_2$ ), 29.66 (CH), 19.89 ( $\text{CH}_3$ ). IR ( $\text{CH}_2\text{Cl}_2$ ,  $\text{cm}^{-1}$ ): 2049, 2002  $\nu(\text{CO})$ . HRMS:  $m/z$  calcd. for  $\text{C}_{18}\text{H}_{25}\text{FeIN}_2\text{O}_2$  [ $\text{M} - \text{I}$ ]<sup>+</sup>, 357.1246; found, 357.1260. Elemental Analysis calcd. (%) for  $\text{C}_{18}\text{H}_{25}\text{FeIN}_2\text{O}_2$  (484.16): C, 44.65; H, 5.20; N, 5.79; found: C, 44.34; H, 5.15; N, 5.69.

**Synthesis of **3e**.** According to a slightly modified Method A, the mixture of base and ligand was directly cannulated into the toluene solution of  $[\text{CpFe}(\text{CO})_2\text{I}]$  (161 mg, 0.53 mmol) by starting from **1e** (157 mg, 0.53 mmol) and  $\text{KOtBu}$  (77 mg, 0.64 mmol). The solvents were removed under reduced pressure, and the crude was used directly for the synthesis of **3e**. Single yellow crystals suitable for X-ray diffraction were obtained by slow diffusion of  $\text{Et}_2\text{O}$  into a  $\text{CH}_2\text{Cl}_2$  solution of the complex.

$^1\text{H}$  NMR (300 MHz,  $\text{CD}_2\text{Cl}_2$ ):  $\delta$  5.31 (s, 5H, Cp), 5.11–5.02 (m, 1H, CH), 4.19 (s, 3H,  $\text{NCH}_3$ ), 3.62–3.52 (m, 1H, CH), 1.62 (d,  $J = 6$  Hz, 6H,  $\text{CH}_3$ ), 1.43 (d,  $J = 6$  Hz, 6H,  $\text{CH}_3$ ).  $^{13}\text{C}\{^1\text{H}\}$  NMR (101 MHz,  $\text{CD}_2\text{Cl}_2$ ):  $\delta$  212.57 (CO), 152 ( $\text{C}_{\text{trz}}-\text{Fe}$ ), 87.31 (Cp), 58.30 (NCH), 46.71 ( $\text{C}_{\text{trz}}$ ), 39.85 ( $\text{NCH}_3$ ), 27.58 (CCH), 23.90 ( $\text{CH}_3$ ), 20.54 ( $\text{CH}_3$ ). IR ( $\text{CH}_2\text{Cl}_2$ ,  $\text{cm}^{-1}$ ): 2042, 1996  $\nu(\text{CO})$ . HRMS:  $m/z$  calcd. for  $\text{C}_{16}\text{H}_{22}\text{FeIN}_2\text{O}$  [ $\text{M} - \text{I}$ ]<sup>+</sup>, 344.1056; found, 344.1050.

Elemental Analysis calcd. (%) for  $C_{16}H_{22}FeIN_3O_2$  (471.01): C, 40.79; H, 4.71; N, 8.92; found: C, 40.55; H, 4.25; N, 8.90.

**Synthesis of 3f.** According to Method B, complex **3f** was afforded as a yellow powder (58 mg, 39%) by starting from **2f** (66 mg, 0.22 mmol) and  $[CpFe(CO)_2]I$  (77 mg, 0.25 mmol). Analytical data agree with those reported for this compound.<sup>27</sup>

**Synthesis of 4a.** According to Method A, the crude product was started from **2a** (45 mg, 0.32 mmol) and  $[Cp^*Fe(CO)_2]I$  (106 mg, 0.28 mmol), extracted with  $CH_2Cl_2$ , and filtrated through a short pad of silica; the volatiles were removed by reduced pressure to yield the complex **4a** as a yellow powder (52 mg, 39%). Single crystals suitable for X-ray diffraction were obtained by slow diffusion of  $Et_2O$  to a  $CH_2Cl_2$  solution of the complex.

$^1H$  NMR (400 MHz,  $CD_2Cl_2$ ):  $\delta$  7.42 (s, 2H,  $H_{im}$ ), 3.83 (s, 6H,  $NCH_3$ ), 1.84 (s, 15H,  $Cp^*-CH_3$ ).  $^{13}C\{^1H\}$  NMR (101 MHz,  $CD_2Cl_2$ ):  $\delta$  214.20 (CO), 172.90 ( $C_{im}-Fe$ ), 127.17 ( $C_{im}-H$ ), 99.45 ( $C_{Cp^*Ar}$ ), 36.86 ( $NCH_3$ ), 10.45 ( $Cp^*-CH_3$ ). IR ( $CH_2Cl_2$ ,  $cm^{-1}$ ): 2027, 1977  $\nu(CO)$ . HRMS:  $m/z$  calcd. for  $C_{17}H_{23}FeIN_2O_2$   $[M - I]^+$ , 343.1103; found, 343.1106. Elemental Analysis calcd. (%) for  $C_{17}H_{23}FeIN_2O_2$  (470.01): C, 43.43; H, 4.93; N, 5.96; found: C, 42.93; H, 4.68; N, 5.93.

**Synthesis of 4b.** According to Method A, complex **4b** was afforded as a yellow powder (140 mg, 62%) by starting from **1b** (140 mg, 0.47 mmol),  $KOtBu$  (67 mg, 0.55 mmol), and  $[Cp^*Fe(CO)_2]I$  (160 mg, 0.43 mmol).

According to Method B, complex **4b** was afforded as a yellow powder (141 mg, 71%) by starting from **2b** (75 mg, 0.38 mmol) and  $[Cp^*Fe(CO)_2]I$  (142 mg, 0.38 mmol). Single crystals suitable for X-ray diffraction were obtained by slow diffusion of  $Et_2O$  to a  $CH_2Cl_2$  solution of the complex.

$^1H$  NMR ( $CD_2Cl_2$ , 400 MHz):  $\delta$  7.44 (s, 2H,  $Im$ ), 4.53 (sept,  $J$  = 7.0 Hz, 2H, CH), 1.82 (s, 15H,  $Cp^*-CH_3$ ), 1.61, 1.46 (d,  $J$  = 6.1 Hz, 12H,  $CH_3$ ).  $^{13}C\{^1H\}$  NMR ( $CD_2Cl_2$ , 101 MHz):  $\delta$  214.03 (CO), 169.14 ( $C_{im}-Fe$ ), 122.59 ( $C_{im}-H$ ), 99.45 ( $C_{Cp^*Ar}$ ), 55.15 (CH), 24.91, 24.47, 23.24 ( $CH_3$ ), 10.24 ( $Cp^*-CH_3$ ). IR ( $CH_2Cl_2$ ,  $cm^{-1}$ ): 2024, 1977  $\nu(CO)$ . HRMS:  $m/z$  calcd. for  $C_{21}H_{31}FeIN_2O_2$   $[M - I]^+$ , 399.1729; found, 399.1731. Elemental Analysis calcd. (%) for  $C_{21}H_{31}FeIN_2O_2$  (526.24): C, 47.93; H, 5.94; N, 5.32; found: C, 47.55; H, 5.83; N, 4.89.

**General Procedure for the Preparation of Complexes 5 and 6.** Complex **3** or **4** was dissolved in  $CH_2Cl_2$  and irradiated with a high intensity UV lamp at 365 nm for 16 h. The resulting green solution was concentrated to  $\sim 2$  mL and layered with dry hexane. After 24 h, the solution was filtered and evaporated to dryness to yield a dark green solid.

**Synthesis of 5c.** According to the general procedure from **3c** (308 mg, 0.64 mmol), complex **5c** (189 mg, 64%) was afforded. Single crystals suitable for X-ray diffraction were obtained by dissolving the crude in  $CH_2Cl_2$  (2 mL) and layering with dry hexanes.

$^1H$  NMR (300 MHz,  $CD_2Cl_2$ ,  $-20^\circ C$ ):  $\delta$  7.20, 7.06 (br, 2H,  $H_{im}$ ), 4.90 (dd,  $J$  = 13.7, 8.9 Hz, 1H,  $CH_2$ ), 4.43 (s, 5H,  $Cp-H$ ), 4.34 (dd,  $J$  = 13.6, 7.1 Hz, 1H,  $CH_2$ ), 4.19–4.01 (m, 2H,  $CH_2$ ), 2.39–2.21 (m, 1H, CH), 2.10–2.03 (m, 1H, CH), 1.06 (d,  $J$  = 6.6 Hz, 3H,  $CH_3$ ), 1.00 (dd,  $J$  = 11.9, 6.8 Hz, 6H,  $CH_3$ ), 0.74 (d,  $J$  = 6.6 Hz, 3H,  $CH_3$ ).  $^{13}C\{^1H\}$  NMR (101 MHz,  $CD_2Cl_2$ ):  $\delta$  224.50 (CO), 184.14 ( $C_{im}-Fe$ ), 122.77 ( $C_{im}-H$ ), 80.30 ( $C_{Cp}$ ), 60.68, 58.39 ( $NCH_2$ ), 29.51, 29.25 (CH), 19.95, 19.87, 19.72, 19.56 ( $CH_3$ ). IR ( $CH_2Cl_2$ ,  $cm^{-1}$ ): 1934  $\nu(CO)$ . HRMS:  $m/z$  calcd. for  $C_{17}H_{25}FeIN_2O$   $[M - I]^+$ , 329.1304; found, 329.1311. Elemental Analysis calcd. (%) for  $C_{17}H_{25}FeIN_2O$  (456.15): C, 44.76; H, 5.52; N, 6.14; found: C, 44.58; H, 5.37; N, 6.25.

**Synthesis of 5e.** The general procedure starting from **3e** afforded complex **5e** (50 mg, 21%, overall yield from **1e**). Single crystals suitable for X-ray diffraction were obtained by dissolving the crude in  $CH_2Cl_2$  (2 mL) and layering with dry hexanes.

$^1H$  NMR (400 MHz, toluene- $d_6$ ,  $65^\circ C$ ):  $\delta$  6.42–6.08, 4.52–4.27 (broad, 2H, CH), 4.20 (s, 5H, Cp), 3.11 (s,  $CH_3$ ), 1.53–1.35, 1.08–0.99, 0.95–0.83 (broad, 12H,  $CH_3$ ). Major rotamer (60%):  $^1H$  NMR (400 MHz,  $CD_2Cl_2$ ,  $-25^\circ C$ ):  $\delta$  6.36 (sept, 6.7 Hz, 1H, NCH), 3.96 (sept, 7.3 Hz, 1H, CH), 4.39 (s, 5H, Cp), 4.01 (s,  $CH_3$ ), 1.65, 1.49–

1.45 (d, 6.7 Hz, 6H,  $NCCH_3$ ), 1.38, 1.17 (d, 7.3 Hz, 6H,  $CH_3$ ).  $^{13}C\{^1H\}$  NMR (101  $CD_2Cl_2$ ,  $-25^\circ C$ ):  $\delta$  225.07 (CO), 163.57 ( $C_{tr}-Fe$ ), 151.25 ( $C_{tr}-C$ ), 79.94 (Cp), 57.89 (NCH), 38.19 ( $NCH_3$ ), 26.84 (CCH), 24.25, 23.32, 20.39, 20.03 ( $CH_3$ ). Minor rotamer (40%):  $^1H$  NMR (400 MHz,  $CD_2Cl_2$ ,  $-25^\circ C$ ):  $\delta$  5.40 (sept, 6.7 Hz, 1H, NCH), 4.71 (sept, 7.3 Hz, 1H, CH), 4.40 (s, 5H, Cp), 4.03 (s,  $CH_3$ ), 1.55, 1.35 (d, 6.7 Hz, 6H,  $NCCH_3$ ), 1.49–1.45, 1.27 (d, 7.3 Hz, 6H,  $CH_3$ ).  $^{13}C\{^1H\}$  NMR (101  $CD_2Cl_2$ ,  $-25^\circ C$ ):  $\delta$  225.17 (CO), 164.52 ( $C_{tr}-Fe$ ), 153.60 ( $C_{tr}-C$ ), 80.24 (Cp), 56.17 (NCH), 38.29 ( $NCH_3$ ), 28.21 (CCH), 23.45, 23.30, 20.37, 19.99 ( $CH_3$ ). IR ( $CH_2Cl_2$ ,  $cm^{-1}$ ): 1928  $\nu(CO)$ . HRMS:  $m/z$  calcd. for  $C_{15}H_{22}FeN_3O$   $[M - I]^+$ , 316.1107; found, 316.1099. Elemental Analysis calcd. (%)  $C_{15}H_{22}FeIN_3O$  (456.15): C, 40.66; H, 5.00; N, 9.48; found: C, 41.16; H, 5.10; N, 9.52.

**Synthesis of 6a.** The imidazolium carboxylate **2a** (72 mg, 0.51 mmol) and  $[Cp^*Fe(CO)_2]I$  (267 mg, 0.70 mmol) were suspended in dry toluene (5 mL) and stirred at  $80^\circ C$  for 16 h under the exclusion of light. After cooling to room temperature, the precipitate was collected by filtration and washed with toluene (2  $\times$  3 mL). According to the general procedure, complex **6a** was afforded as a green powder (39.4 mg, 40%). Single crystals suitable for X-ray diffraction were obtained by dissolving the product in  $CH_2Cl_2$  (2 mL) and layering with dry hexanes.

$^1H$  NMR (400 MHz,  $CD_2Cl_2$ ):  $\delta$  7.08, 6.98 (d,  $J$  = 4.0 Hz, 2H,  $H_{im}$ ), 4.04, 3.86 (s, 6H,  $NCH_3$ ), 1.69 (s, 15H,  $Cp^*-CH_3$ ).  $^{13}C\{^1H\}$  NMR (101 MHz,  $CD_2Cl_2$ ):  $\delta$  226.66 (CO), 191.15 ( $C_{im}-Fe$ ), 124.69, 124.47 ( $C_{im}-H$ ), 89.51 ( $C_{Cp^*Ar}$ ), 43.08 ( $NCH_3$ ), 39.27 ( $NCH_3$ ), 10.65 ( $Cp^*-CH_3$ ). IR ( $CH_2Cl_2$ ,  $cm^{-1}$ ): 1914  $\nu(CO)$ . HRMS:  $m/z$  calcd. for  $C_{16}H_{23}FeIN_2O$   $[M - I]^+$ , 315.1155; found, 315.1154. Elemental Analysis calcd. (%) for  $C_{16}H_{23}FeIN_2O$  (442.12) ( $Et_2O$ ) 0.2%: C, 44.16; H, 5.51; N, 6.13; found: C, 43.81; H, 6.05; N, 6.27.

**Synthesis of 6b.** According to the general procedure, complex **6b** was afforded as a green powder (80 mg, 60%) from **4b** (140 mg, 0.27 mmol). Single crystals suitable for X-ray diffraction were obtained by dissolving the product in  $CH_2Cl_2$  (2 mL) and layering with dry hexanes.

$^1H$  NMR:  $\delta$  7.17, 7.07 (d,  $J$  = 4.0 Hz, 2H,  $Im$ ), 5.63–5.42, 5.25–4.97 (m, 2H, CH), 1.66 (s, 15H,  $Cp^*-CH_3$ ), 1.62, 1.48, 1.42, 1.38 (d,  $J$  = 6.4 Hz, 12H,  $CH_3$ ).  $^{13}C\{^1H\}$  NMR (101 MHz,  $CD_2Cl_2$ ):  $\delta$  119.90, 119.35 ( $C_{im}-H$ ), 88.99 ( $C_{Cp^*Ar}$ ), 53 (CH), 24.89, 24.87, 23.35 ( $CH_3$ ), 10.89 ( $Cp^*-CH_3$ ). IR ( $CH_2Cl_2$ ,  $cm^{-1}$ ): 1910  $\nu(CO)$ . HRMS:  $m/z$  calcd. for  $C_{20}H_{31}FeIN_2O$   $[M - I]^+$ , 371.1780; found, 371.1775. Elemental Analysis calcd. (%) for  $C_{20}H_{31}FeIN_2O$  (498.08): C, 48.21; H, 6.27; N, 5.62; found: C, 48.25; H, 6.30; N, 6.07.

**Synthesis of 7c.** The imidazolium salt **1c** (334 mg, 1.02 mmol) and  $KOtBu$  (155 mg, 1.28 mmol) were suspended in dry THF (10 mL). After 1 h of stirring at room temperature, the mixture was added to a suspension of  $[CpFe(CO)_2]I$  (159 mg, 0.85 mmol) in dry toluene (30 mL) and stirred at room temperature for 1 h under the exclusion of light. The precipitate was collected by filtration, washed with ether (2  $\times$  10 mL), taken up in  $CH_2Cl_2$ , and filtrated through a short pad of silica. All volatiles were removed under reduced pressure. The residue was dissolved in  $CH_2Cl_2$ , and  $AgPF_6$  (212 mg, 0.84 mmol) was added. After 1 h of stirring at room temperature under the exclusion of light, the mixture was filtrated through a short pad of silica and the solvents were removed under reduced pressure. The residue was dissolved in MeCN (15 mL) and irradiated with a high intensity UV lamp at 365 nm for 40 h. The volatiles were removed under reduced pressure. Single crystals suitable for X-ray diffraction were obtained by dissolving the product in  $CH_2Cl_2$  and layering with dry hexanes (202 mg, 47%).

$^1H$  NMR (400 MHz,  $CD_2Cl_2$ ):  $\delta$  7.29 (s, 2H,  $H_{im}$ ), 4.71 (s, 5H, Cp), 4.16–4.11 (m, 2H,  $CH_2$ ), 3.96–3.91 (m, 2H,  $CH_2$ ), 2.28 (s, 3H,  $CH_3CN$ ), 2.18 (m, 2H, CH), 1.02, 0.96 (d,  $J$  = 6.6 Hz, 12H,  $CH_3$ ).  $^{13}C\{^1H\}$  NMR (101 MHz,  $CD_2Cl_2$ ):  $\delta$  220.05 (CO), 176.56 ( $C_{im}-Fe$ ), 134.61 ( $CNCH_3$ ), 124.24 ( $C_{im}-H$ ), 82.59 (Cp), 58.43 ( $CH_2$ ), 29.73 (CH), 20.02 ( $CH_3$ ), 5.16 ( $CH_3CN$ ). IR ( $CH_2Cl_2$ ,  $cm^{-1}$ ): 1980  $\nu(CO)$ . HRMS:  $m/z$  calcd. for  $C_{19}H_{28}FeN_3O$   $[M - PF_6]^+$ , 370.1576; found, 370.1575. Elemental Analysis calcd. (%) for  $C_{19}H_{28}F_6FeN_3OP$



(S15.26): C, 44.29; H, 5.48; N, 8.16; found: C, 44.33; H, 5.66; N, 8.11.

**Typical Procedure for Hydrosilylation Catalysis.** A solution of 4-nitrobenzaldehyde (0.5 mmol), phenylsilane (74  $\mu$ L; 0.6 mmol), and hexamethylbenzene (8.1 mg; 0.05 mmol) or 1,3,5-trimethoxybenzene (8.4 mg; 0.05 mmol) in 1,2-dichloroethane (2.0 mL) was stirred at 60 °C for 10 min under an N<sub>2</sub> atmosphere. The iron complex was added from a stock solution (0.5 mL, 0.01 M, 5  $\mu$ mol), and aliquots were taken at specific times, diluted with CDCl<sub>3</sub>, and analyzed by <sup>1</sup>H NMR spectroscopy.

**Crystallographic Details.** All measurements were made on an Oxford Diffraction SuperNova area-detector diffractometer<sup>62</sup> using mirror optics, monochromated Mo K $\alpha$  radiation ( $\lambda$  = 0.71073 Å), and Al filtering.<sup>63</sup> The unit cell constants and an orientation matrix for data collection were obtained from a least-squares refinement of the setting angles of reflections in the range of  $2.0^\circ < \theta < 27.9^\circ$ . A total of 728 frames were collected using  $\omega$  scans with 8 + 8 s exposure time, a rotation angle of 1.0° per frame, a crystal–detector distance of 65.0 mm, and  $T$  = 173(2) K. Data reduction was performed using the CrysAlisPro<sup>62</sup> program. The intensities were corrected for Lorentz and polarization effects, and a numerical absorption correction based on Gaussian integration over a multifaceted crystal model was applied. Data collection and refinement parameters are presented in the **Supporting Information**. The structure was solved by direct methods using SHELXT,<sup>64</sup> which revealed the positions of the non-hydrogen atoms of the title compound. All non-hydrogen atoms were refined anisotropically. All H atoms were placed in geometrically calculated positions and refined using a riding model where each H atom was assigned a fixed isotropic displacement parameter with a value equal to 1.2 Uequiv of its parent atom (1.5 Uequiv for methyl groups). Refinement of the structure was carried out on  $F^2$  using full-matrix least-squares procedures, which minimized the function  $\sum w(F_o^2 - F_c^2)^2$ . The weighting scheme was based on counting statistics and included a factor to downweigh the intense reflections. All calculations were performed using the SHELXL-2014/7<sup>65</sup> program in OLEX2.<sup>66</sup> Further crystallographic details are compiled in **Tables S2–S6**. Crystallographic data for the structures of all compounds reported in this paper have been deposited with the Cambridge Crystallographic Data Centre (CCDC) as supplementary publication numbers 2072827 (3c), 2072824 (3e), 2072829 (4a), 2072831 (4b), 2072826 (5c), 2072828 (5e), 2072825 (6a), 2072832 (6b), and 2072830 (7c).

## ■ ASSOCIATED CONTENT

### SI Supporting Information

The Supporting Information is available free of charge at <https://pubs.acs.org/doi/10.1021/acs.organomet.1c00200>.

Experimental procedures for ligands, NMR spectra, free energy calculations, cyclic voltammetry, crystallographic details, buried volume calculations, and catalytic and mechanistic details (PDF)

## Accession Codes

CCDC 2072824–2072832 contain the supplementary crystallographic data for this paper. These data can be obtained free of charge via [www.ccdc.cam.ac.uk/data\\_request/cif](http://www.ccdc.cam.ac.uk/data_request/cif), or by emailing [data\\_request@ccdc.cam.ac.uk](mailto:data_request@ccdc.cam.ac.uk), or by contacting The Cambridge Crystallographic Data Centre, 12 Union Road, Cambridge CB2 1EZ, UK; fax: +44 1223 336033.

## ■ AUTHOR INFORMATION

### Corresponding Author

Martin Albrecht – Department of Chemistry & Biochemistry, University of Bern, 3012 Bern, Switzerland; [orcid.org/0000-0001-7403-2329](https://orcid.org/0000-0001-7403-2329); Email: [martin.albrecht@dcb.unibe.ch](mailto:martin.albrecht@dcb.unibe.ch)

## Authors

Pamela V. S. Nylund – Department of Chemistry & Biochemistry, University of Bern, 3012 Bern, Switzerland  
Nathalie C. Ségaud – Department of Chemistry & Biochemistry, University of Bern, 3012 Bern, Switzerland;  
[orcid.org/0000-0002-9221-1416](https://orcid.org/0000-0002-9221-1416)

Complete contact information is available at:  
<https://pubs.acs.org/doi/10.1021/acs.organomet.1c00200>

## Notes

The authors declare no competing financial interest.

## ■ ACKNOWLEDGMENTS

We thank the European Research Council (ERC 615653) for generous financial support of our work in this area and the group at Chemical Crystallography of the University of Bern for X-ray analyses.

## ■ REFERENCES

- (1) Bauer, I.; Knölker, H. J. Iron Catalysis in Organic Synthesis. *Chem. Rev.* **2015**, *115*, 3170–3387.
- (2) Bolm, C.; Legros, J.; Le Pailh, J.; Zani, L. Iron-Catalyzed Reactions in Organic Synthesis. *Chem. Rev.* **2004**, *104*, 6217–6254.
- (3) Morris, R. H. Asymmetric Hydrogenation, Transfer Hydrogenation and Hydrosilylation of Ketones Catalyzed by Iron Complexes. *Chem. Soc. Rev.* **2009**, *38*, 2282–2291.
- (4) Zhang, M.; Zhang, A. Iron-Catalyzed Hydrosilylation Reactions. *Appl. Organomet. Chem.* **2010**, *24*, 751–757.
- (5) Du, X.; Huang, Z. Advances in Base-Metal-Catalyzed Alkene Hydrosilylation. *ACS Catal.* **2017**, *7*, 1227–1243.
- (6) Lopes, R.; Royo, B. Iron N-Heterocyclic Carbenes in Reduction Reactions. *Isr. J. Chem.* **2017**, *57*, 1151–1159.
- (7) Wei, D.; Darcel, C. Iron Catalysis in Reduction and Hydrometalation Reactions. *Chem. Rev.* **2019**, *119*, 2550–2610.
- (8) Raya-Barón, A.; Oña-Burgos, P.; Fernández, I. Iron-Catalyzed Homogeneous Hydrosilylation of Ketones and Aldehydes: Advances and Mechanistic Perspective. *ACS Catal.* **2019**, *9*, 5400–5417.
- (9) Yun, J.; Kim, D.; Yun, H. A New Alternative to Stryker's Reagent in Hydrosilylation: Synthesis, Structure, and Reactivity of a Well-Defined Carbene-Copper(Ii) Acetate Complex. *Chem. Commun.* **2005**, *942*, 5181.
- (10) Lopes, R.; Pereira, M. M.; Royo, B. Selective Reduction of Nitroarenes with Silanes Catalyzed by Nickel N-Heterocyclic Carbene Complexes. *ChemCatChem* **2017**, *9*, 3073–3077.
- (11) Hofmann, R. J.; Vlatkovic, M.; Wiesbrock, F. Fifty Years of Hydrosilylation in Polymer Science: A Review of Current Trends of Low-Cost Transition-Metal and Metal-Free Catalysts, Non-Thermally Triggered Hydrosilylation Reactions, and Industrial Applications. *Polymers* **2017**, *9*, 534.
- (12) Bart, S. C.; Lobkovsky, E.; Chirik, P. J. Preparation and Molecular and Electronic Structures of Iron(0) Dinitrogen and Silane Complexes and Their Application to Catalytic Hydrogenation and Hydrosilylation. *J. Am. Chem. Soc.* **2004**, *126*, 13794–13807.
- (13) Wu, J. Y.; Stanzl, B. N.; Ritter, T. A Strategy for the Synthesis of Well-Defined Iron Catalysts and Application to Regioselective Diene Hydrosilylation. *J. Am. Chem. Soc.* **2010**, *132*, 13214–13216.
- (14) Sanagawa, A.; Nagashima, H. Cobalt(0) and Iron(0) Isocyanides as Catalysts for Alkene Hydrosilylation with Hydro-siloxanes. *Organometallics* **2018**, *37*, 2859–2871.
- (15) Hu, M. Y.; He, Q.; Fan, S. J.; Wang, Z. C.; Liu, L. Y.; Mu, Y. J.; Peng, Q.; Zhu, S. F. Ligands with 1,10-Phenanthroline Scaffold for Highly Regioselective Iron-Catalyzed Alkene Hydrosilylation. *Nat. Commun.* **2018**, *9*, 1–12.
- (16) Zhang, M.; Zhang, J.; Ni, X.; Shen, Z. Bis(Phenolate) N-Heterocyclic Carbene Rare Earth Metal Complexes: Synthesis, Characterization and Applications in the Polymerization of n-Hexyl Isocyanate. *RSC Adv.* **2015**, *5*, 83295–83303.

- (17) Kandepe, V. V. K. M.; Cardoso, J. M. S.; Peris, E.; Royo, B. Iron(II) Complexes Bearing Chelating Cyclopentadienyl-N-Heterocyclic Carbene Ligands as Catalysts for Hydrosilylation and Hydrogen Transfer Reactions. *Organometallics* **2010**, *29*, 2777–2782.
- (18) Jiang, F.; Bézier, D.; Sortais, J. B.; Darcel, C. N-Heterocyclic Carbene Piano-Stool Iron Complexes as Efficient Catalysts for Hydrosilylation of Carbonyl Derivatives. *Adv. Synth. Catal.* **2011**, *353*, 239–244.
- (19) Bézier, D.; Jiang, F.; Roisnel, T.; Sortais, J. B.; Darcel, C. Cyclopentadienyl-NHC Iron Complexes for Solvent-Free Catalytic Hydrosilylation of Aldehydes and Ketones. *Eur. J. Inorg. Chem.* **2012**, *2012*, 1333–1337.
- (20) Demir, S.; Gökçe, Y.; Kaloğlu, N.; Sortais, J. B.; Darcel, C.; Özdemir, I. Synthesis of New Iron-NHC Complexes as Catalysts for Hydrosilylation Reactions. *Appl. Organomet. Chem.* **2013**, *27*, 459–464.
- (21) Lopes, R.; Cardoso, J. M. S.; Postigo, L.; Royo, B. Reduction of Ketones with Silanes Catalysed by a Cyclopentadienyl-Functionalised N-Heterocyclic Iron Complex. *Catal. Lett.* **2013**, *143*, 1061–1066.
- (22) Buchgraber, P.; Toupet, L.; Guerschais, V. Syntheses, Properties, and X-Ray Crystal Structures of Piano-Stool Iron Complexes Bearing an N-Heterocyclic Carbene Ligand. *Organometallics* **2003**, *22*, 5144–5147.
- (23) Mercks, L.; Labat, G.; Neels, A.; Ehlers, A.; Albrecht, M. Piano-Stool Iron(II) Complexes as Probes for the Bonding of N-Heterocyclic Carbenes: Indications for  $\pi$ -Acceptor Ability. *Organometallics* **2006**, *25*, 5648–5656.
- (24) Guisado-Barrios, G.; Bouffard, J.; Donnadieu, B.; Bertrand, G. Crystalline 1H-1,2,3-Triazol-5-Ylidenes: New Stable Mesoionic Carbenes (MICs). *Angew. Chem., Int. Ed.* **2010**, *49*, 4759–4762.
- (25) Bouffard, J.; Keitz, B. K.; Tonner, R.; Guisado-Barrios, G.; Frenking, G.; Grubbs, R. H.; Bertrand, G. Synthesis of Highly Stable 1,3-Diaryl-1 H -1,2,3-Triazol-5-Ylidenes and Their Applications in Ruthenium-Catalyzed Olefin Metathesis. *Organometallics* **2011**, *30*, 2617–2627.
- (26) Trnka, T. M.; Morgan, J. P.; Sanford, M. S.; Wilhelm, T. E.; Scholl, M.; Choi, T. L.; Ding, S.; Day, M. W.; Grubbs, R. H. Synthesis and Activity of Ruthenium Alkylidene Complexes Coordinated with Phosphine and N-Heterocyclic Carbene Ligands. *J. Am. Chem. Soc.* **2003**, *125*, 2546–2558.
- (27) Johnson, C.; Albrecht, M. Triazolylidene Iron(II) Piano-Stool Complexes: Synthesis and Catalytic Hydrosilylation of Carbonyl Compounds. *Organometallics* **2017**, *36*, 2902–2913.
- (28) Ohki, Y.; Hatanaka, T.; Tatsumi, K. *J. Am. Chem. Soc.* **2008**, *130* (7), 17174–17186.
- (29) Liang, Q.; Osten, K. M.; Song, D. Iron-Catalyzed Gem-Specific Dimerization of Terminal Alkynes. *Angew. Chem., Int. Ed.* **2017**, *56*, 6317–6320.
- (30) Liang, Q.; Sheng, K.; Salmon, A.; Zhou, V. Y.; Song, D. Active Iron(II) Catalysts toward Gem-Specific Dimerization of Terminal Alkynes. *ACS Catal.* **2019**, *9*, 810–818.
- (31) Liang, Q.; Hayashi, K.; Rabeda, K.; Jimenez-Santiago, J. L.; Song, D. Piano-Stool Iron Complexes as Precatalysts for Gem-Specific Dimerization of Terminal Alkynes. *Organometallics* **2020**, *39*, 2320–2326.
- (32) Rieger, K.; Haslinger, S.; Raba, A.; Högerl, M. P.; Cokoja, M.; Herrmann, W. A.; Kühn, F. E. Chemistry of Iron N-Heterocyclic Carbene Complexes: Syntheses, Structures, Reactivities, and Catalytic Applications. *Chem. Rev.* **2014**, *114*, 5215–5272.
- (33) Royo, B. Cyclopentadienyl-Functionalized n-Heterocyclic Carbene Complexes of Iron and Nickel: Catalysts for Reductions. In *Advances in Organometallic Chemistry and Catalysis*; Pombiero Armando, J. L., Ed.; John Wiley & Sons Inc., 2014; DOI: 10.1016/s1351-4180(14)70389-7.
- (34) Johnson, C.; Albrecht, M. Piano-Stool N-Heterocyclic Carbene Iron Complexes: Synthesis, Reactivity and Catalytic Applications. *Coord. Chem. Rev.* **2017**, *352*, 1–14.
- (35) Voutchkova, A. M.; Appelhans, L. N.; Chianese, A. R.; Crabtree, R. H. Disubstituted Imidazolium-2-Carboxylates as Efficient Precursors to N-Heterocyclic Carbene Complexes of Rh, Ru, Ir, and Pd. *J. Am. Chem. Soc.* **2005**, *127*, 17624–17625.
- (36) Wyer, E.; Gucciardo, G.; Leigh, V.; Müller-Bunz, H.; Albrecht, M. Comparison of Carbene and Imidazole Bonding to a Copper(I) Center. *J. Organomet. Chem.* **2011**, *696*, 2882–2885.
- (37) Albrecht, M.; Maji, P.; Häusel, C.; Monney, A.; Müller-Bunz, H. N-Heterocyclic Carbene Bonding to Cobalt Porphyrin Complexes. *Inorg. Chim. Acta* **2012**, *380*, 90–95.
- (38) Ségaud, N.; McMaster, J.; Van Koten, G.; Albrecht, M. Imidazolylidene Cu(II) Complexes: Synthesis Using Imidazolium Carboxylate Precursors and Structure Rearrangement Pathways. *Inorg. Chem.* **2019**, *58*, 16047–16058.
- (39) Shapovalov, S. S.; Tikhonova, O. G.; Skabitskii, I. V.; Kolos, A. V.; Sakharov, S. G.; Torubaev, Y. V. Oxidation of Iron Complex with NHC Ligand with Molecular Iodine. *Russ. J. Inorg. Chem.* **2019**, *64*, 1418–1423.
- (40) Shapovalov, S. S.; Tikhonova, O. G.; Grigor'eva, M. O.; Skabitskii, I. V.; Simonenko, N. P. Metal Complexes with the N-Heterocyclic Ligand: Synthesis, Structures, and Thermal Decomposition. *Russ. J. Coord. Chem.* **2019**, *45*, 706–711.
- (41) Naumann, S.; Schmidt, F. G.; Schowner, R.; Frey, W.; Buchmeiser, M. R. Polymerization of Methyl Methacrylate by Latent Pre-Catalysts Based on CO<sub>2</sub>-Protected N-Heterocyclic Carbenes. *Polym. Chem.* **2013**, *4*, 2731.
- (42) Akita, M.; Terada, M.; Tanaka, M.; Morooka, Y. Some Additional Aspects of Versatile Starting Compounds for Cationic Organoiron Complexes: Molecular Structure of the Aqua Complex [(H<sub>5</sub>-C<sub>5</sub>Me<sub>4</sub>Et)Fe(CO)<sub>2</sub>(OH<sub>2</sub>)]BF<sub>4</sub> and Solution Behavior of the THF Complex [(H<sub>5</sub>H—C<sub>5</sub>R<sub>5</sub>)Fe(CO)<sub>2</sub>(THF)]BF<sub>4</sub>. *J. Organomet. Chem.* **1996**, *510*, 255–261.
- (43) Günther, H. *NMR-Spektroskopie*; Georg Thieme Verlag Stuttgart, 1973.
- (44) Mathew, P.; Neels, A.; Albrecht, M. 1,2,3-Triazolylidenes as Versatile Abnormal Carbene Ligands for Late Transition Metals. *J. Am. Chem. Soc.* **2008**, *130* (130), 13534–13535.
- (45) Faliyev, L.; Cao, Z.; Petta, A.; Serra, L.; Poater, A.; Oliva, R.; Scarano, V.; Cavallo, L. Towards the Online Computer-Aided Design of Catalytic Pockets. *Nat. Chem.* **2019**, *11*, 872–879.
- (46) Gutsulyak, D. V.; Kuzmina, L. G.; Howard, J. A. K.; Vyboishchikov, S. F.; Nikonov, G. I. Cp(Pri<sub>2</sub>MeP)FeH<sub>2</sub>SiR<sub>3</sub>: Nonclassical Iron Silyl Dihydride. *J. Am. Chem. Soc.* **2008**, *130*, 3732–3733.
- (47) Lam, Y. C.; Nielsen, R. J.; Goddard, W. A.; Dash, A. K. The Mechanism for Catalytic Hydrosilylation by Bis(Imino)Pyridine Iron Olefin Complexes Supported by Broken Symmetry Density Functional Theory. *Dalt. Trans.* **2017**, *46*, 12507–12515.
- (48) Smith, P. W.; Dong, Y.; Tilley, T. D. Efficient and Selective Alkene Hydrosilylation Promoted by Weak, Double Si-H Activation at an Iron Center. *Chem. Sci.* **2020**, *11*, 7070–7075.
- (49) Bleith, T.; Gade, L. H. Mechanism of the Iron(II)-Catalyzed Hydrosilylation of Ketones: Activation of Iron Carboxylate Precatalysts and Reaction Pathways of the Active Catalyst. *J. Am. Chem. Soc.* **2016**, *138*, 4972–4983.
- (50) Metsänen, T. T.; Gallego, D.; Szilvási, T.; Driess, M.; Oestreich, M. Peripheral Mechanism of a Carbonyl Hydrosilylation Catalysed by an SiN<sub>2</sub> Iron Pincer Complex. *Chem. Sci.* **2015**, *6*, 7143–7149.
- (51) O'Connor, J. M.; Casey, C. P. Ring-Slippage Chemistry of Transition-Metal Cyclopentadienyl and Indenyl Complexes. *Chem. Rev.* **1987**, *87*, 307–318.
- (52) No product was observed by <sup>1</sup>H NMR, nor was any precipitation observed. No precipitation was observed in the NMR tube, nor were any new signals observed, indicative of a product formation.
- (53) Hamon, J.-R.; Hamon, P.; Toupet, L.; Costuas, K.; Saillard, J.-Y. Classical and Non-Classical Iron Hydrides: Synthesis, NMR Characterisation, Theoretical Investigation and X-Ray Crystal Structure of the Iron(IV) Dihydride [Cp\*Fe(Dppe)(H)<sub>2</sub>] + BF<sub>4</sub>-. *C. R. Chim.* **2002**, *5*, 89–98.



- (54) Li, H.; Misal Castro, L. C.; Zheng, J.; Roisnel, T.; Dorcet, V.; Sortais, J. B.; Darcel, C. Selective Reduction of Esters to Aldehydes under the Catalysis of Well-Defined NHC-Iron Complexes. *Angew. Chem., Int. Ed.* **2013**, *52*, 8045–8049.
- (55) Becker, B.; Corriu, R. J. P.; Guérin, C.; Henner, B. J. L. Hypervalent Silicon Hydrides: Evidence for Their Intermediacy in the Exchange Reactions of Di- and Tri-Hydrogenosilanes Catalysed by Hydrides (NaH, KH and LiAlH<sub>4</sub>). *J. Organomet. Chem.* **1989**, *369*, 147–154.
- (56) Docherty, J. H.; Dominey, A. P.; Thomas, S. P. Nucleophile Induced Ligand Rearrangement Reactions of Alkoxy- and Arylsilanes. *Tetrahedron* **2019**, *75*, 3330–3335.
- (57) Bellamy, L. J. *The Infra-Red Spectra of Complex Molecules*, 3rd ed.; Chapman and Hall Ltd.: London, 1975.
- (58) Analysis of this reaction mixture by <sup>1</sup>H NMR spectroscopy revealed the same changes in chemical shifts as observed by <sup>1</sup>H NMR spectroscopic reaction monitoring (Figure S74 cf. Figure S63).
- (59) Warner, M. C.; Verho, O.; Bäckvall, J. E. CO Dissociation Mechanism in Racemization of Alcohols by a Cyclopentadienyl Ruthenium Dicarbonyl Catalyst. *J. Am. Chem. Soc.* **2011**, *133*, 2820–2823.
- (60) Stewart, B.; Nyhlen, J.; Martín-Matute, B.; Bäckvall, J. E.; Privalov, T. A Computational Study of the CO Dissociation in Cyclopentadienyl Ruthenium Complexes Relevant to the Racemization of Alcohols. *Dalt. Trans.* **2013**, *42*, 927–934.
- (61) Connelly, N. G.; Geiger, W. E. Chemical Redox Agents for Organometallic Chemistry. *Chem. Rev.* **1996**, *96*, 877–910.
- (62) Oxford Diffraction Ltd. *CrysAlisPro* (Version 1.171.40.39a); Oxford Diffraction Ltd., Yarnton, Oxfordshire, UK, 2018; pp 279–288.
- (63) Macchi, P.; Bu, H.; Chimpri, A. S.; et al. Low-Energy Contamination of Mo Microsource X-Ray Radiation: Analysis and Solution of the Problem. *J. Appl. Crystallogr.* **2011**, *44*, 763–771.
- (64) Sheldrick, G. M. Research Papers SHELXT - Integrated Space-Group and Crystal- Structure Determination Research Papers. *Acta Crystallogr., Sect. A: Found. Adv.* **2015**, *71*, 3–8.
- (65) Sheldrick, G. M. Crystal Structure Refinement with SHELXL. *Acta Crystallogr., Sect. C: Struct. Chem.* **2015**, *71*, 3–8.
- (66) Dolomanov, O. V.; Bourhis, L. J.; Gildea, R. J.; Howard, J. A. K.; Puschmann, H. OLEX2: A Complete Structure Solution, Refinement and Analysis Program. *J. Appl. Crystallogr.* **2009**, *42*, 339–341.